Properties of liquid and solid ^{4}He

P. A. Whitlock and D. M. Ceperley*
Courant Institute of Mathematical Sciences, New York University, New York, New York 10012

G. V. Chester
Laboratory of Atomic and Solid State Physics, Cornell University, Ithaca, New York 14853

M. H. Kalos
Courant Institute of Mathematical Sciences, New York University, New York, New York 10012
(Received 12 October 1978)

A Monte Carlo method is used to compute the properties of the fluid and crystal phases of the Lennard-Jones model of ^{4}He at absolute zero. The method yields exact results subject only to statistical sampling errors. The energy, structure factor, and momentum distribution are calculated at several densities in both phases. In addition, in the crystal phase we have carried out a detailed study of the single-particle distribution function. The densities at which melting and freezing occurs are determined. In both phases perturbative estimates of the three-body Axilrod-Teller potential are computed. Overall the agreement with experiment is good to excellent. However there are significant discrepancies between the computed and experimental equations of state. We believe this is due to the inadequacy of the Lennard-Jones potential.

I. INTRODUCTION

The properties of the fluid and crystal states of ^{4}He, at absolute zero, have been extensively studied by numerical methods for more than ten years. This has nearly always been done by variational methods using a trial function consisting of a product of two-body correlation functions for the fluid phase. The same kind of product times a product of one-body functions has been used for the crystal phase. The evaluation of the many-body integrals that arise in the variational computations has been carried out either by Monte Carlo integration or by hypernetted-chain (HNC) methods.[1] ^{4}He is the only simple, boson system that can be readily studied in the laboratory and it therefore is interesting in its own right. Furthermore, simplified models of condensed helium have recently become benchmark problems in the general study of quantum many-body systems.[2] Many theorists now take the view that a method, for example the HNC integral equation, is subjected to an important and stringent test when it is applied to fluid ^{3}He and ^{4}He at absolute zero.

At the same time, it has become clear that while the simple product trial function is a valuable guide to the properties of such systems it is sufficiently in error, in calculations of the energy and structure, to preclude quantitative comparison with experiment and critical evaluation of the He-He interatomic potential. In addition, understanding the source of the deficiencies of the product form is of considerable interest and, we believe, is likely to improve in a substantial way ones ability to treat other quantum systems, notably ^{3}He.

The error resulting from the use of product trial functions in the calculation of the energy of the fluid states of ^{4}He was first estimated by Kalos.[3] He found an energy 0.7 °K deeper than the value of −6 °K obtained from variational calculations.[1,4,5] This result was confirmed by additional numerical studies by Kalos, Levesque, and Verlet[6]; the latter will be henceforth referred to as KLV. Recently some light has been cast upon this discrepancy by two studies[5,7] in which explicit three-body correlations were introduced into trial functions. Approximate evaluation of the change in the variational energy was in fair agreement with the 0.7 °K per particle, found by Kalos[3] and by KLV. These results strongly suggest that the major inadequacy in the usual trial functions is the absence of explicit three-body correlations.

For these reasons we decided that it was timely to do a careful study of the properties of the fluid and

crystal phases of ^{4}He at zero temperature. We use the Green's-function Monte Carlo method to integrate numerically the Schrödinger equation and obtain exact energy values for a finite system with periodic boundary conditions. The results of Kalos[3] were computed for 32 particles only, while those of KLV were derived from computations on a hard-sphere system by using a perturbation method. One motive for this work was to assess the validity of the KLV perturbation estimates. Another, as suggested above, was to provide reliable numerical results to which other, more approximate, methods could be compared. Since it has been used in nearly all other studies, our calculations were carried out with the Lennard-Jones potential having the de Boer–Michels parameters,[8]

$$V(r)=4\epsilon[(\sigma/r)^{12}-(\sigma/r)^{6}]\ ,$$
$$\epsilon=10.22\ ^{\circ}\mathrm{K}\ , \tag{1.1}$$
$$\sigma=2.556\ \text{Å}\ .$$

The earlier work[3,6] had suggested that this potential was in better agreement with experimental energy and structure than had been thought previously. We wished to study this and other comparisons with experiment more carefully. This will help determine which, if any, alternative potentials[9] are better than the original Lennard-Jones. In addition we were interested in assessing whether the properties predicted by the Lennard-Jones potential were accurate enough to justify its use in calculating other properties, for example the surface energy and structure of liquid and crystal helium.

Our calculations were carried out using the Green's-function Monte Carlo method. Henceforth we shall refer to this as the GFMC method. This method makes it possible to compute exactly the energy and other properties of a Bose system, subject to statistical sampling errors. Section II of this paper gives a brief summary of the method. A more thorough treatment of the GFMC method has been given by Ceperley and Kalos[10] along with a comprehensive review of Monte Carlo calculations in the quantum many-body problem, (see also Refs. 3 and 6). Here we give special attention to the technical questions that are most important for the present calculations, especially the ever-vexing problems of assuring reliable results and of estimating their errors.

Section III presents our results for the fluid phase at absolute zero, including the calculated equation of state, structure function, and momentum density at densities ranging from 0.9 to 1.3 times the experimental equilibrium density. The effect on the energy of the Axilrod-Teller three-body potential[11] is estimated as well. These data are compared with the earlier variational, the hard-sphere perturbation results, and, where possible, with experiment.

A corresponding presentation of the properties of the face-centered-cubic crystal phase is given in Sec. IV with densities ranging from the melting density to approximately 1.25 times that density. Results for metastable fcc crystals are also given below the freezing density. In addition to data on the equation of state and radial distribution function, we discuss the distribution of single-particle displacements from lattice sites and the melting-freezing transition. We thereby draw some conclusions about the nature of the crystalline ground state.

Section V is devoted to a summary and our view of the prospectives for future work on the numerical study of helium stystem along with some comments on various two-body potentials that have been proposed for the He-He interaction.

II. COMPUTATIONAL METHODS

The basic aim of our paper is to give numerical results for the lowest energy eigenvalues of the Hamiltonian

$$\mathcal{H}=-(\hbar^2/2m)\sum_{i=1}^{N}\nabla_i^2+\sum_{i<j}V(r_{ij})\ , \tag{2.1}$$

as a function of the density of the system and for both fluid and crystal states. Here $V(r)$ is the Lennard-Jones potential quoted in the Introduction [Eq. (1.1)]. Various expectations with respect to the ground-state eigenfunction will be discussed as well. One such expectation is the perturbative effect of the Axilrod-Teller three-body potential which is discussed in Appendix A.

In this section we give a summary of the computational methods, emphasizing our assessments of the reliability, and the numerical and statistical accuracy of our results. In general the errors themselves are quoted along with results in Secs. III and IV.

A. Variational methods

We stated in the Introduction that most of the numerical studies of the properties of quantum fluids at absolute zero have been carried out by variational methods. In such calculations, a trial function for N particles,

$$\psi_T(r_1,r_2,\cdots,r_N)\equiv\psi_T(R)$$

is assumed to be

$$\psi_T(R)=\prod_{i<j}f(r_{ij})\ , \tag{2.2}$$

where f is a function whose form is arbitrary but with parameters that may be varied.

For crystal phases, the commonly used trial function is

$$\psi_T(R) = \prod_{i<j} f(r_{ij}) \prod_m \phi(r_m - s_m) , \quad (2.3)$$

where the s_m are the lattice sites appropriate to the crystal order being studied. Although Eq. (2.3) is not symmetric as required for a Bose system, it has been shown[12] that the resulting error in the energy is very small.

Variational estimates of the energy are obtained from the equation

$$E_T = \frac{\int \psi_T^* \mathcal{H} \psi_T \, dR}{\int |\psi_T|^2 \, dR} . \quad (2.4)$$

The true ground-state eigenvalue is $E_0 \leq E_T$. The functional form and parameters used in f and ϕ are varied so as to minimize the energy. Expectation values are calculated with respect to that ψ_T which yields the lowest energy.

Many computations of this type have been carried out by using the Metropolis method[1,10,13] to sample $|\psi_T(R)|^2$ and thus form Monte Carlo estimates of E_T and of other expectation values. As discussed below, trial functions used in variational studies published by other researchers are used as "importance functions" to accelerate the convergence of the iterative scheme (GFMC) we use to solve the Schrödinger equation. Populations of points $\{R\}$ drawn from the probability density $|\psi_T(R)|^2$ are suitable for starting such iterations. Lastly, variational expectation values are essential in the extrapolation procedure discussed below which is used to calculate ground-state properties from the GFMC configurations. The trial functions used for extrapolations are the same as those used to accelerate the convergence. For these reasons we have repeated variational calculations described in the literature. Further discussion including an enumeration of the particular forms of ψ_T which were used, is given in Sec. II B.

B. Green's-function Monte Carlo method (GFMC)

It is possible to devise a number of schemes which integrate the Schrödinger equation by Monte Carlo methods. All successful methods are fundamentally similar and rest upon the analogy between the wave equation for the ground state and diffusion equations. The particular algorithm which has thus far proved most successful in treating many-body problems uses the Green's function for the operator $\mathcal{H} + V_0$ (for constant V_0)[14] to put the Schrödinger equation in integral form. The required Green's function is the solution of a diffusion problem and hence is also the expectation of the density generated by any of a class of random walks. Monte Carlo methods may therefore be used to sample the Green's function. At the same time a related Monte Carlo process carries out the integrations that are required in the iteration of the integral equation equivalent to Schrödinger's equation. This Green's-function Monte Carlo method makes it possible to compute the exact energy and other properties of a Bose system, subject to statistical sampling errors.

More specifically we seek the lowest-energy solution ψ_0 and its eigenvalue E_0 of the equation

$$\mathcal{H}\psi = E\psi . \quad (2.5)$$

Let $G(R,R')$ satisfy

$$(\mathcal{H} + V_0) G(R,R') = \delta(R - R') \quad (2.6)$$

with the same boundary conditions as are appropriate for $\psi_0(R)$. Then Eq. (2.6) is used to put Eq. (2.5) in integral form

$$\psi_0(R) = (E_0 + V_0) \int G(R,R') \psi_0(R') \, dR' . \quad (2.7)$$

Now the ground-state wave function for a Bose system and $G(R,R')$ are both non-negative; $\psi_0(R)$ and useful approximations to it may be treated as probability density functions. The Green's function $G(R,R')$ may be regarded as a density function for choosing a point R conditional on R'. Let a population of points $\{R'\}$ be drawn from $\psi^{(1)}(R') = \psi_T(R')$ and new points $\{R\}$ be sampled from $(E_t + V_0) G(R,R')$ for each R', where E_t is a trial eigenvalue. Then the expected density, averaged over the population $\{R'\}$, of new points in a neighborhood of R is

$$\psi^{(2)}(R) = (E_t + V_0) \int G(R,R') \psi^{(1)}(R') \, dR' . \quad (2.8)$$

Since a population of new points is produced (we call this a new generation) it is clearly possible to iterate the process as many times as may be required, leading to the recurrence relationship

$$\psi^{(n+1)}(R) = (E_t + V_0) \int G(R,R') \times \psi^{(n)}(R') \, dR' . \quad (2.9)$$

Since we are concerned with a system of N particles with periodic boundary conditions, the Hamiltonian has a discrete spectrum and the iteration described by Eq. (2.9) converges to the ground-state wave function $\psi_0(R)$.

A crucial aspect of the method is the ability to sample $G(R,R')$. To describe fully the algorithm we use would take us too far afield. A comprehensive treatment of this and other aspects of the Green's-function Monte Carlo method is given in Ref. 10.

One technical matter with which we must concern ourselves is an importance sampling transformation whereby the convergence and efficiency of the GFMC may be improved. In this variant of the basic

Monte Carlo procedure, an approximation to the exact ground-state wave function is introduced into the iteration. The trial functions, $\psi_T(R)$, used in variational studies are appropriate as such importance functions. The transformation is simply to multiply Eq. (2.9) by $\psi_T(R)$ to obtain

$$\psi_T(R)\psi^{(n+1)}(R) = (E_t+V_0)\int \frac{\psi_T(R)G(R,R')}{\psi_T(R')}[\psi_T(R')\psi^{(n)}(R')]\,dR' . \tag{2.10}$$

It is natural to let the initial distribution from which points are drawn to start the iteration be $|\psi_T(R)|^2$, the same distribution sampled in carrying out a variational calculation. In addition the modified kernel $\psi_T(R)G(R,R')/\psi_T(R')$ must be sampled. How this is done and the advantages of importance sampling are also described in Ref. 10. Here we note only that the asymptotic distribution is now $\psi_T(R)\psi_0(R)$ and that as ψ_T approaches $\psi_0(R)$ the energy may be inferred with no statistical error.

We now discuss a number of technical points which are pertinent; in particular the estimation of the energy and other observables from a combination of variational and GFMC results. We summarize also the errors involved and how these may be estimated or bounded.

C. Estimation of the ground-state energy

Because the exact ground-state energy is not known in advance, a trial energy is used in Eq. (2.9). If the trial eigenvalue E_t is larger than E_0, then the functions $\psi^{(n)}$ will grow in normalization with n, which implies a growth of the average population of configurations with generations. If E_t is less than E_0 the population of configurations decreases. A "growth" estimator for the ground-state energy may be calculated from the change in population size,

$$E_0+V_0 \cong \frac{(E_t+V_0)\int \psi_T(R)\psi^{(n)}(R)\,dR}{\int \psi_T(R)\psi^{(n+1)}(R)\,dR}$$

$$= (E_t+V_0)N_n/N_{n+1} , \tag{2.11}$$

where N_n is the number of configurations in the nth generation. The estimator in Eq. (2.11) is biased even after convergence since the expected value of a quotient is not the quotient of the expected values. An asymptotically unbiased estimator for the energy can be devised by defining a "mixed expectation" for an operator F,

$$\langle F\rangle_M = \frac{\int \psi_0(R)F\psi_T(R)\,dR}{\int \psi_0(R)\psi_T(R)\,dR} , \tag{2.12}$$

then the mixed expectation for the energy is

$$E_M = \frac{\int \psi_0(R)\mathcal{H}\psi_T(R)\,dR}{\int \psi_0(R)\psi_T(R)\,dR} . \tag{2.13}$$

We call this a variational estimator; except for sampling and convergence errors it gives the exact energy on the average. As $\psi_T(R)$ approaches $\psi_0(R)$ the estimator of Eq. (2.13) gives precisely E_0, independent of the values of R which occur in the random walk so that the Monte Carlo error is zero. The statistical error in the "growth estimator" is larger than that in the "variational estimator"; we therefore always report the latter. The growth estimator is however used to test convergence and numerical consistency and to bound possible bias.

There are several sources of error in the results we report. Each determination of the ground-state energy by the GFMC method was iterated for 300–500 generations. Various estimates of the energy were used to determine when $\psi^{(n)}$ had converged to ψ_0. If one substitutes for $\psi^{(n)}$ in Eq. (2.10) an expansion in ψ_K, the eigenfunctions of $\mathcal{H}+V_0$, it is easy to infer that the coefficient of ψ_K decays as $[(E_0+V_0)/(E_K+V_0)]^n$ in n iterations. Thus the convergence to ψ_0 is asymptotically geometric and is faster when V_0 is made as small as practical. In our calculations the value of V_0 was set to +30 °K per particle and we observed that upon starting with configurations from a variational Monte Carlo calculation, convergence required about 30 generations. Accordingly, about 100 generations were discarded before performing any averages. We have deduced that the bias contributed to the ground-state energy by this procedure is approximately 0.015 °K per particle which is less than other errors.

TABLE I. Size dependence of the energy (E_2). The first column gives the density in reduced units, E_2 is in degrees Kelvin per particle.

$\rho\sigma^3$	Phase	N	E_2
0.328	liquid	32	−6.74 ± 0.04
		64	−6.66 ± 0.04
		128	−6.64 ± 0.02
0.365	liquid	32	−6.84 ± 0.03
		64	−6.83 ± 0.05
0.468	crystal	32	−5.41 ± 0.07
		108	−5.52 ± 0.05

An unavoidable fact about any Monte Carlo procedure is that one samples only a finite number of points in the random walk. In addition, in the GFMC method, the random walk tends to be correlated over about 20 generations. If a fluctuation occurs, its effect is likely to persist for a part of the calculation. We have estimated the standard error associated with the energy by dividing a run into six or more blocks with 30–40 generations in each block and computed the error from the energies of each block. This process assumed that the blocks are statistically independent which is not strictly true if the random walk is correlated. The error calculation was tested by discarding every other block and recomputing the error; the value increased by roughly $2^{1/2}$ as if the blocks were independent. We believe, therefore, that our estimates of the statistical errors are representative of the actual errors.

We have also evaluated the dependence of the energy calculation on the size of the system studied. Table I summarizes the results of GFMC calculations on liquid ^{4}He at a density of $0.3283\sigma^{-3}$ for $N=32$, 64, and 128 particles and at a density of $0.3648\sigma^{-3}$ for $N=32$ and 64 particles. Except for the energy calculated with $N=32$ at $\rho=0.3283\sigma^{-3}(=0.9\rho_0)$ there is no indication of any size dependence; all other results agree within one standard error. The effect seen at the lowest density may be associated with a Van der Waals loop for the metastable fluid phase. We conclude that the uncertainty owing to the use of 64 particles in fluid calculations is less than about 0.04 °K. Table I also shows a comparison of energies from GFMC calculations of crystalline ^{4}He at $\rho=0.468\sigma^{-3}$ for $N=32$ and 108 particles. The energies agree within their statistical errors.[15] The error in using 108 body results is less than 0.05 °K.

By changing the importance function ψ_T used in Eq. (2.10), the accuracy of the computational method is subjected to a stringent test. In principle, the computed ground-state energy and all other properties should be unaffected by a change in the importance function, and this is generally what we observe. The importance function was varied in several ways; for example, with a McMillan[1] type function

$$\psi_T=\prod_{i<j} f(r_{ij}) ,$$
$$u(r)=-\ln f(r)=\tfrac{1}{2}(b/r)^5 , \tag{2.14}$$

GFMC calculations were done with both the optimal variational parameter b and a nonoptimum value. The importance function was changed completely by using pseudopotentials of a form proposed by de Michelis and Reatto[4];

$$u(r)=(b/r)^5\exp[-(r/r_0)^2]-A\{E(\lambda-r)+E(r-\lambda)\exp[-(r-\lambda)^2/\Lambda^2]\}+C\exp[-(r-d)^2/D^2] , \tag{2.15}$$

TABLE II. Dependence of various quantities on the importance function. N gives the number of particles used in the simulation, b and C are parameters in the importance function defined in the text. All energies are in degrees Kelvin per particle, lengths are in units of σ, and n_0 is the fraction of particles in the zero-momentum state.

				Liquid			
$\rho\sigma^3$	N	Importance Function	b	E_2	$\langle V\rangle$	$g(r)$ at peak	n_0
0.3648	64	McMillan	1.20	−6.81 ± 0.07	−20.35 ± 0.10	1.323 ± 0.020	···
0.3648	64	McMillan	1.161	−6.83 ± 0.05	−20.48 ± 0.15	1.326 ± 0.016	0.113 ± 0.005
0.3648	64	Reatto α	···	−6.65 ± 0.04	−20.28 ± 0.23	1.337 ± 0.015	0.116 ± 0.001
0.3648	64	Reatto β	···	−6.85 ± 0.02	−20.44 ± 0.18	1.339 ± 0.018	0.111 ± 0.005

					Crystal			
$\rho\sigma^3$	N	Importance Function	b	C	E_2	$\langle V\rangle$	$g(r)$ at peak	$\langle r^2\rangle$
0.526	108	McMillan	1.096	6.5	−4.74 ± 0.03	31.87 ± 0.10	1.596 ± 0.018	0.1272 ± 0.0024
0.526	108	McMillan	1.140	5.0	−4.80 ± 0.06	32.15 ± 0.28	1.609 ± 0.033	0.1225 ± 0.0051

where $E(x)$ is the step function. The expression in Eq. (2.15) has a repulsive Gaussian term which was introduced to simulate the effects of three-particle terms in the wave function. Calculations were performed employing two sets of the Reatto parameters. The first, called α in Ref. 4, gave the minimum energy of -5.96 ± 0.2 °K in their variational calculations

$$\left.\begin{array}{ll} A=0.5, & c=0.2 \\ \lambda=1.5, & d=1.8 \\ \Lambda=1.0, & D=0.6 \end{array}\right\} \alpha .$$

The second, β, gave the best structure factor $S(k)$ among the sets studied and an energy of -5.65 ± 0.2 °K. The parameters were

$$\left.\begin{array}{ll} A=0.6, & c=0.25 \\ \lambda=1.25, & d=2.0 \\ \Lambda=1.15, & D=0.6 \end{array}\right\} \beta .$$

All crystal calculations used a ψ_T of the form (2.3) with McMillan's pseudopotential, Eq. (2.14), and

$$\phi(r)=\exp(-\tfrac{1}{2}Ar^2) . \tag{2.16}$$

The parameters b and A were taken from the work of Hansen and Levesque.[16] To study the effect of changing ψ_T for GFMC calculations in the crystal state we changed both b and A from their optimal values. The results of all such changes of the importance function are summarized in Table II. It is clear from this table that the properties of the ground state are insensitive within their statistical errors to reasonable variations of the form of ψ_T. However, the error and the rate of convergence are affected by the choice of importance function. For example, the GFMC calculation employing the Reatto β function converged faster than that using the McMillan function and showed a variance for the energy about seven times smaller for given computing time. The energy obtained with the Reatto α importance function appears to be a significant exception to the insensitivity of results to ψ_T, lying outside the errors of all other results. Two comments are appropriate. The series of calculations upon which the result is based was rather short, being abandoned when it was clear that the importance function was a poor one. Thus, although it appeared to converge, more computation would have been required to be sure. Second, our own variational calculation gave an energy of -5.25 ± 0.1 °K (in contradiction to the published value of Ref. 4), indicating that this function is not a "reasonable" choice of ψ_T. It is possible, by a very poor choice of importance function and short runs, to obtain misleading results.

Another source of error lies in the calculation of $V(r)$ and derivatives of $u(r)$ from tables rather than from the explicit functional forms. The effect of this was examined by comparing the energy calculated from a set of configurations using the tables and separately the continuous functions. Another measure of this error is the difference between "growth" estimates of the energy which use no tables and "variational" estimates which do. From these we estimate the error owing to the use of tables in the energy to be much less than 0.01 °K.

D. Other ground-state properties

In addition to the ground-state energy, both the variational and the GFMC methods can yield much other information. It is a great advantage of computer simulations that one can gather information about many microscopic properties from a single calculation. Of primary interest in liquids is the radial distribution function

$$g(\vec{r})=(1/N\rho)\sum_{i\neq j}\langle\delta(\vec{r}_i-\vec{r}_j-\vec{r})\rangle \tag{2.17}$$

and its Fourier transform, the structure factor

$$S(\vec{k})-1=(\rho/2)\int d\vec{r}\,e^{i\vec{k}\cdot\vec{r}}[g(\vec{r})-1] . \tag{2.18}$$

There has been continuing interest in $n(\vec{k})$, the momentum density of liquid ^{4}He to determine whether a momentum condensate is present in the ground state. The Fourier transform of $n(\vec{k})$ is

$$\begin{aligned}\rho_1(\vec{r}) &= \int d\vec{k}\,e^{i\vec{k}\cdot\vec{r}}n(\vec{k}) \\ &= \langle\psi_0(\vec{r}_i+\vec{r})/\psi_0(\vec{r}_i)\rangle \end{aligned} \tag{2.19}$$

and the fraction of particles in the zero-momentum state is given by[17]

$$n_0=\lim_{r\to\infty}\rho_1(r) . \tag{2.20}$$

In the solid, the correlation function of most interest is the one-body density for displacements from a lattice site,

$$\rho(\vec{r})=\langle\delta(\vec{r}_i-\vec{s}_i-\vec{r})\rangle .$$

The degree of isotropy of $\rho(\vec{r})$ can be investigated by observing the distribution of the displacements in various directions from the lattice site.

The above quantities are somewhat more difficult to obtain from the Monte Carlo calculation than the ground-state energy and thus the errors are more difficult to bound. Here, also, changing the importance function acts as a strong check on the errors. Table II and additional data given below show that the physical properties we have discussed are indeed independent of the importance function.

As was described earlier, the importance sampled GFMC calculation yields points chosen from the asymptotic distribution $\psi_T\psi_0$. Any average computed from the GFMC configurations is a "mixed" average [cf. Eq. (2.12)]; however, we are really interested in ground-state expectation values taken with respect to

ψ_0. One method of extracting the exact result is to assume that the trial function ψ_T is close to the ground-state wave function,

$$\psi_T = \psi_0 + \delta\psi \ .$$

Then if one computes any expectation from the variational and the GFMC "mixed" wave functions, a linear extrapolation may be made, defining

$$\langle F\rangle_{\rm ex} = 2\langle F\rangle_M - \langle F\rangle_T \ . \tag{2.21}$$

Here $\langle F\rangle_M$ is defined by Eq. (2.12) and $\langle F\rangle_T$ is the expectation value computed with ψ_T. The extrapolation of Eq. (2.21) will give the ground-state property $\langle F\rangle_0$ to order δ^2. An example of extrapolation is shown in Figs. 1 and 2 for $S(k)$ and $n(k)$ with several different trial functions. The structure of the first peak of $S(k)$ is considerably sharpened by the extrapolation process. Also, the different trial functions give values for $S(k)$ which are in agreement after extrapolation, although the "mixed" estimates are different. The results for $n(k)$ in Fig. 2 were all obtained by Fourier transforming a smoothed $\rho_1(r)$ obtained from Eq. (2.19). This procedure is not reliable for $k < \sigma^{-1}$ because of the noise in $\rho_1(r)$ at large r. The standard error at $k = 0.56\sigma^{-1}$ is about 25%. For $k > \sigma^{-1}$ the standard errors, estimated from fluctuations in sequential runs, increase from about 3% to about 15% at $k = 5\sigma^{-1}$. The differences between the results obtained from different importance functions are not statistically significant. The discrepancy at $k = 1.12\sigma^{-1}$ is less than two standard errors, and values at small k are sensitive to slowly decaying density fluctuations. For $\vec{k}$ in the reciprocal lattice of the periodicity box $n(\vec{k})$ may be obtained from a mixed expectation of

$$\frac{e^{i\vec{k}\cdot\vec{r}_l}\psi_T(\vec{r}_1, \cdots, \vec{r}_l+\vec{r}_1, \cdots, \vec{r}_N)}{\psi_T(\vec{r}_1, \cdots, \vec{r}_N)} \ .$$

Such data, having somewhat larger errors than those quoted above, were obtained and are discussed in Sec. III C. They agree within statistics with the $n(k)$ obtained by Fourier transform.

We performed two GFMC calculations for a crystal at a density of $\rho = 0.526\sigma^{-3}$ in which the importance parameters, b and A, were different. The change in the variational results was significant, producing a 16% shift in the mean square displacement from lattice sites. Nevertheless the GFMC method should be able to converge to the same answer; the agreement shown in Table II confirms the consistency of our calculations and the validity of the extrapolation method for these expectations.

An alternative method of computing the exact value of any property is to use weights derived from the GFMC calculation as explained in Ref. 10. The advantage of this method is that no assumption of

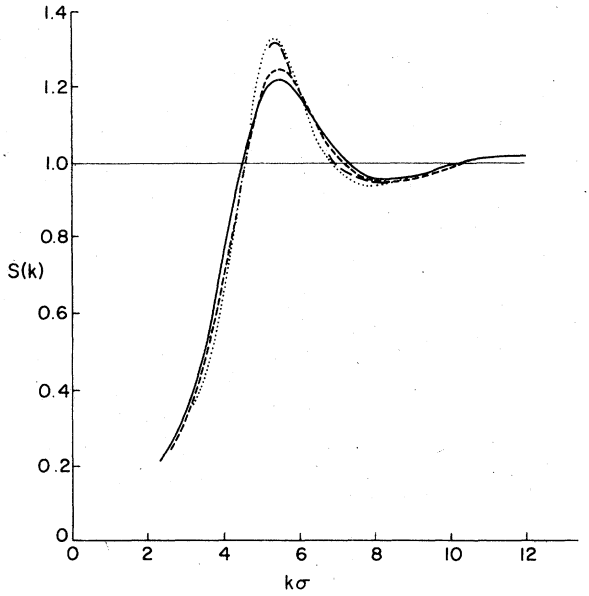

FIG. 1. Extrapolation of the structure function $S(k)$. The solid curve gives $S(k)$ for the McMillan function calculated variationally. The dashed curve gives the results for the Reatto β function calculation variationally. The curve composed of long dashes and the dotted curve give the corresponding results extrapolated from the GFMC results.

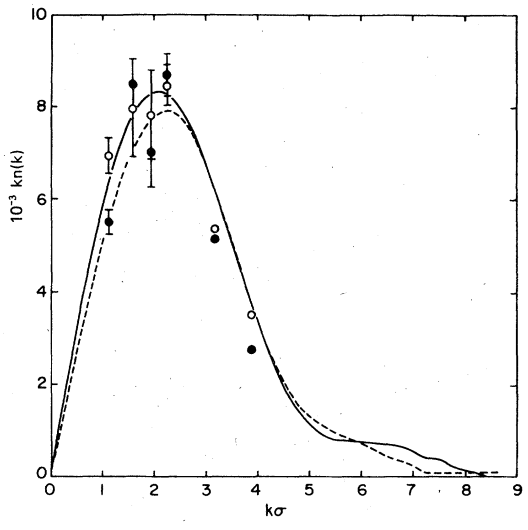

FIG. 2. Momentum distribution function obtained by extrapolation of the GFMC results. The solid curve was obtained using the McMillan function for importance sampling the dashed curve from the Reatto β function. The differences between the two curves is not satistically significant.

linear extrapolation is made. These weights can be obtained from estimates of the asymptotic population size resulting from different configurations. In practice one can only determine approximate weights after some finite number of generations and the statistical error of the weight grows rapidly with that number. In Fig. 3 we show a series of graphs for $g(r)$ obtained at $\rho\sigma^3=0.3283$ and $N=128$. The succession includes the variational $g(r)$, the "mixed" $g(r)$, which effectively uses weights obtained after zero iterations, values obtained with 20 generation weights, and the "extrapolated" $g(r)$. The last is seen to be a plausible extrapolation of the others. In other comparisons, values obtained by "extrapolation" are consistent within statistical errors with those obtained from weights. In general the former are easier to compute and have smaller errors so that we will always report such results below.

III. PROPERTIES OF THE FLUID PHASE

In this section we present all the properties we have computed for the fluid phase. These include the equation of state, pressure, compressibility, structure factor, and momentum distribution. Wherever possible these results are compared with experimental data. Since all previous numerical studies of the Lennard-Jones system have been based on the variational principle, we have made extensive comparisons between this work and our own. In addition, we have compared our results with the perturbative results obtained by KLV.[6]

A. Equation of state in the fluid phase

Energy eigenvalues were computed at five densities in the fluid phase. The eigenvalues we obtained were then corrected by adding to them a perturbation estimate of the contribution from the Axilrod-Teller three-body potential[11] as given in Eq. (A1) of Appendix A. Our estimates are 6–10% larger than those obtained by Murphy and Barker[11] who used a variational Jastrow function to compute an estimate of $\langle V_3\rangle$. The most likely cause of this is that our configurations contain explicit three-body correlations which are not present in the configurations generated by a Jastrow wave function. Our results for $\langle V_3\rangle$ are always positive and therefore raise our estimates of the energy.

Another correction to the energy arises from the long-range correlations produced by the zero-point motion of the phonons. Our method is briefly described in Appendix B. At all densities in the fluid

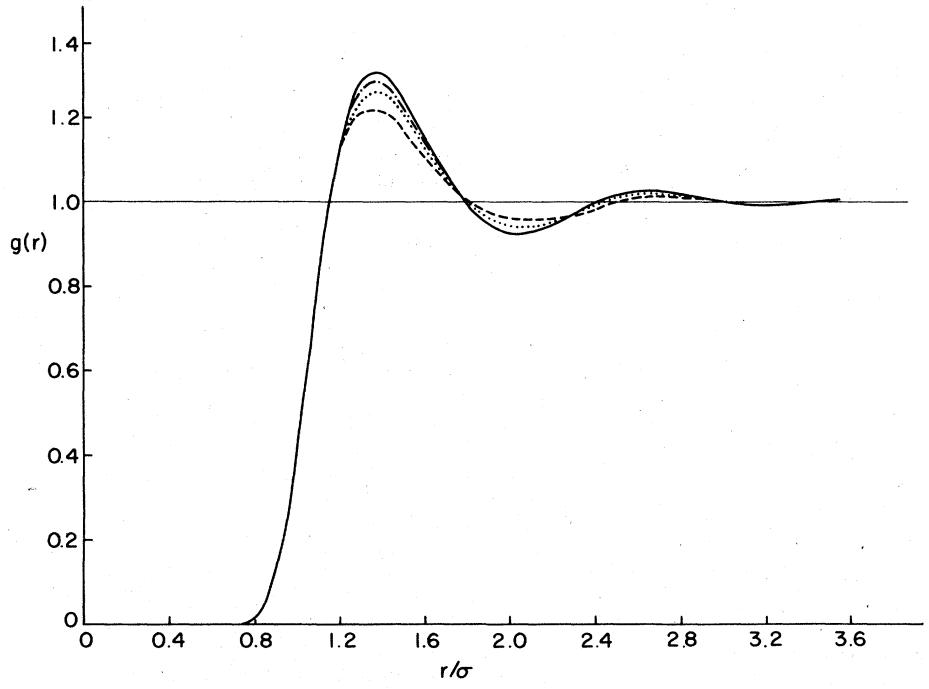

FIG. 3. Radial distribution function $g(r)$ computed by different methods. The dashed curve is the variational $g(r)$, the dotted curve is the "mixed" $g(r)$, the dashed and dotted curve is computed from 20 generation weights and the solid curve is obtained by the extrapolation procedure explained in the text.

phase we find that they are completely negligible, being less than 0.001 °K per particle at ρ_0. This conclusion contradicts that of KLV[6]; the present result is correct as discussed in Appendix B.

In Table III we display our results for the energy at five densities from 0.9 to 1.343 ρ_0, where ρ_0 is the *experimental* equilibrium density.

Column two E_2 gives the GFMC value for the eigenvalue at the given density, $\langle V_3 \rangle$ gives the perturbation estimate of the three-body potential, and E is our value for the total energy. We have estimated our errors in E_2 in the way described in Sec. II C and find them to be less than one percent.

These values for E_2 are independent of the importance function used in the GFMC calculation; see Sec. II C. We also find that our results are independent of the size of the system simulated. We therefore have considerable confidence in the values we have found for E_2 and E.

The tabulated values of the energy may be compared with the experimental values.[18] We see from Table III that from 1.0 to 1.2 ρ_0 there is a roughly constant discrepancy. Our energies are approximately 0.45 °K per particle higher than the experimental values. Since our numerical errors are small and the three-body potential yielded only a small correction to E_2, we believe that the source of this discrepancy must be the Lennard-Jones potential. We will discuss this point in more detail in Sec. V.

We have fitted our five energies E to a cubic polynomial,

$$\frac{E}{N} = A + B\left(\frac{\rho-\bar{\rho}_0}{\bar{\rho}_0}\right)^2 + C\left(\frac{\rho-\bar{\rho}_0}{\bar{\rho}_0}\right)^3 . \tag{3.1}$$

The parameters were found to have the values

$$A = -6.688 \pm 0.016, \quad B = 14.5 \pm 2.5,$$

$$C = -1.2 \pm 7.8, \quad \bar{\rho}_0 = 0.3646 \pm 0.0030 .$$

The errors quoted were determined from the errors in the energies. Note, however, that statistical fluctuations in the parameters are not independent. Errors in other functions which depend upon A, B, C, and $\bar{\rho}_0$ were computed taking account of the correlations.

Within the estimated error, $\bar{\rho}_0$ is identical with the experimental value $\rho_0 = 0.3648\sigma^{-3}$. The ground-state energy per particle is thus equal to our value of E at ρ_0. It is gratifying that the GFMC method yields such a good value for the equilibrium density. All previous variational work has produced equilibrium densities which were too low by at least 10%. Figure 4 shows our GFMC results and the experimental values for the energy. The smooth curve through our results is obtained from Eq. (3.1).

From this formula we have computed the pressure $p(\rho)$ and velocity of sound $C(\rho)$ as a function of the density

$$p(\rho) = \rho^2 \frac{\partial E}{\partial \rho} = \left(\frac{\rho}{\bar{\rho}_0}\right)^2 \left[2B(\rho-\bar{\rho}_0) + \left(\frac{3C}{\bar{\rho}_0}\right)(\rho-\bar{\rho}_0)^2\right], \tag{3.2}$$

$$mC^2(\rho) = \frac{\partial p}{\partial \rho} = \frac{\rho}{\bar{\rho}_0}\left\{2B\frac{3\rho}{\bar{\rho}_0-2} + 6C \times \left[2\left(\frac{\rho}{\bar{\rho}_0}\right)^2 - 3\left(\frac{\rho}{\bar{\rho}_0}\right)+1\right]\right\}. \tag{3.3}$$

A summary of our results for p and C is given in Table IV along with experimental data[18] and they are shown graphically in Figs. 5 and 6. At 1.1 ρ_0 and 1.2 ρ_0 the discrepancies in p are 3 and 12%, respectively. The computed values of the velocity of sound are of comparable quality: at ρ_0, C is but 3% off the experiment while at 1.2 ρ_0 the disagreement is 13%. The

TABLE III. Energies in the fluid phase. The first column gives the density in reduced units, E_2 is the eigenvalue computed using the Lennard-Jones potential, $\langle V_3 \rangle$ is the perturbation estimate of V_3, $E = E_2 + \langle V_3 \rangle$, and E_{exp} is the experimental value of the energy taken from Ref. 18. All energies are in degrees Kelvin per particle. The experimental value for the equilibrium density is given by $\rho\sigma^3 = 0.3648$.

$\rho\sigma^3$	E_2	$\langle V_3 \rangle$	E	E_{exp}
0.328	−6.662 ± 0.035	0.121 ± 0.002	−6.54 ± 0.035	···
0.365	−6.848 ± 0.018	0.157 ± 0.004	−6.69 ± 0.018	−7.14
0.401	−6.743 ± 0.033	0.206 ± 0.002	−6.54 ± 0.033	−7.00
0.438	−6.386 ± 0.072	0.258 ± 0.002	−6.13 ± 0.072	−6.53
0.490	−5.362 ± 0.079	0.343 ± 0.003	−5.02 ± 0.079	···

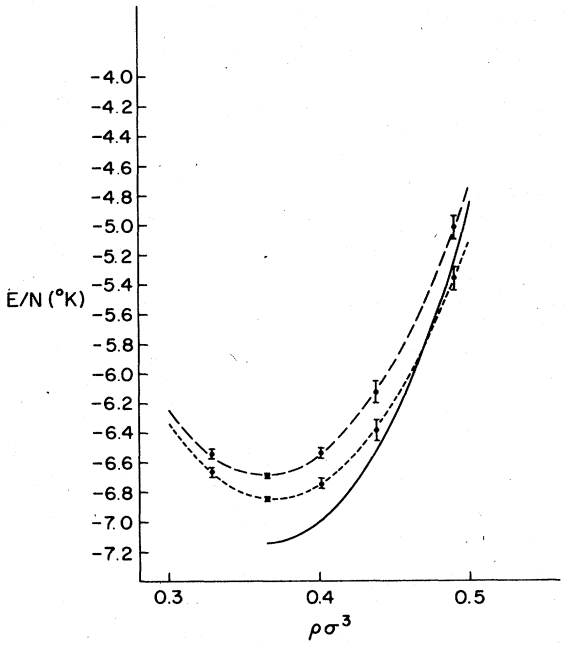

FIG. 4. Ground-state energy as a function of the density for the fluid phase. The solid curve represents the experimental data from Ref. 18. The lower dashed curve represents the GFMC results using only the Lennard-Jones potential and the upper dashed curve includes the perturbation estimate of the three-body potential V_3. The points with error bars represent the data from the GFMC calculation.

errors given for p and C were computed as indicated above; the correlations in the errors of the parameters of Eq. (3.1) reduce the errors of p and C. The pressure may either be calculated from Eq. (3.2) p, or directly from the virial theorem, p_v. The two values should be identical at any given density.[19] Unfortunately the virial pressure requires the estimation of the small difference of two integrals $\int r^{-m} g(r) r^2 \, dr$. We find that "variational" and "mixed" estimates of p_v differ markedly. Thus the extrapolation procedure defined in Eq. (2.21) cannot be applied with confidence to test the consistency of p and p_v.

In Table V we display our values for E_2, $\langle V \rangle$, and $\langle T \rangle$. Here $\langle V \rangle$ is the ground-state expectation value of the Lennard-Jones potential and $\langle T \rangle$ is the expectation value of the kinetic energy. While $\langle V \rangle$ can be accurately extrapolated by the method of Sec. II C, $\langle T \rangle$ does not extrapolate well. The values of $\langle T \rangle$ in Table V are thus defined as $E_2 - \langle V \rangle$. We believe that $\langle T \rangle$ is much more difficult to compute than E_2 or $\langle V \rangle$ because it contains derivatives of the wave function.

Table V reveals a difficulty in computing the energy of liquid ^{4}He: $\langle T \rangle$ and $\langle V \rangle$ are both much larger than E_2. The energy E_2 is thus a consequence of a rather delicate cancellation between the kinetic and potential energy. There have recently been published[20] experimental estimates of $\langle T \rangle$; we will compare our results with these in Sec. III C.

From this discussion we conclude that the GFMC method can yield accurate energies for the Lennard-Jones system. The three-body potential terms are small in the fluid phase. The discrepancy between our results and experiment is almost certainly due to inadequacies in the Lennard-Jones potential. While our results for the pressure and velocity of sound are reasonably satisfactory, the rather large errors in them can only be corrected by either more accurate computations or by computations at additional values of the density.

Several years ago, Kalos, Levesque, and Verlet[6] published the results of a GFMC study of the Bose hard-sphere system. They showed that it was possible to take their results for the hard-sphere system and by a perturbation technique compute the properties of the Lennard-Jones system. The spirit of this work was very similar to the use of the hard-sphere system as a reference system in classical statistical

TABLE IV. Pressure and velocity of sound. The first column gives the density in reduced units, p is in atmospheres, the speed of sound in meters per second, and the experimental data are taken from Ref. 18.

$\rho\sigma^3$	p	p_{exp}	c	c_{exp}
0.365	4.265×10^{-2}	0	245.8 ± 21.0	238.2
0.380	3.934 ± 0.932	3.802	264.7 ± 14.9	266.4
0.401	10.388 ± 1.22	10.667	290.54 ± 8.74	306.2
0.420	17.070 ± 1.198	18.375	312.5 ± 13.4	341.6
0.438	24.360 ± 1.160	27.367	333.1 ± 23.7	375.6
0.473	41.544 ± 3.852	50.565	372.5 ± 49.9	444.3

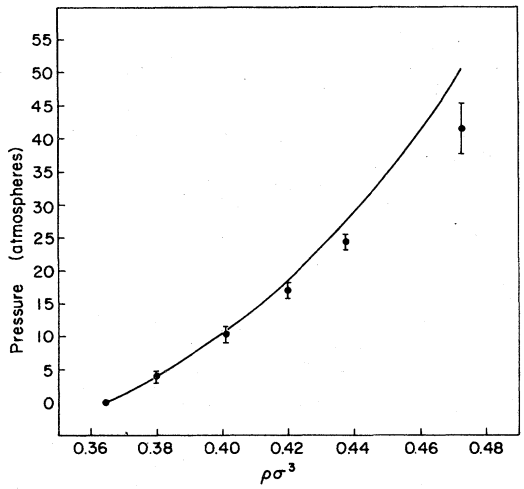

FIG. 5. Comparison of the pressure from the GFMC results and the experimental data of Ref. 18. The solid line represents the experimental results. The points with error bars are the GFMC results.

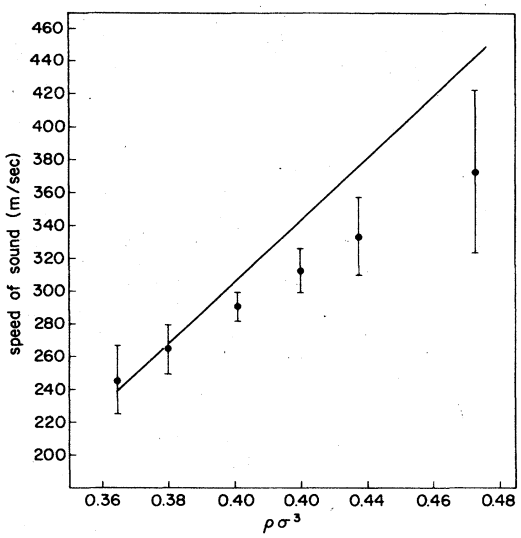

FIG. 6. Comparison of the speed of sound from the GFMC results with the experimental data from Ref. 18. The solid curve represents the experimental data, the points with error bars are the GFMC results.

mechanics.[21] Their results for the energy of the Lennard-Jones system were not given at the densities for which we have computed E_2. To make as accurate a comparison as possible we have used an equation of the form of Eq. (3.1) to compute values of E_2 for $\rho\sigma^3$ equal to 0.341 and 0.416; the values for which the perturbation results were published. The constants A', B', C', and $\bar{\rho}_0'$ used in the polynomial were those found by fitting our values of E_2 — no three-body corrections were incorporated as they are irrelevant for this comparison. We find that at these densities our energies are −6.75 °K per particle and −6.60 °K, respectively as compared with the perturbation values of −6.84 °K and −6.13 °K. We can conclude that the use of the hard-sphere system as a reference system may well be a satisfactory approach for computing the thermodynamic properties of the fluid states of the Lennard-Jones system.

We now give a brief discussion of the variational work that has been performed on the Lennard-Jones system. Our aim is to show what can be learned by comparing our exact GFMC results with those found variationally.

Several types of variational work can be distinguished. Two are of particular interest to us. First, those which are based on variational functions of the product or Jastrow form,[1]

$$\psi_T = \prod_{i<j} f(r_{ij}) \ .$$

In this trial function there are no explicit three-body correlations. Second, two calculations have been published[5,7] which contain explicit three-body correlations in addition to the usual two-body terms.

TABLE V. Energy (E_2), the mean kinetic and potential energies. The first column gives the density in reduced units, $E_2 = \langle T \rangle + \langle V \rangle$. All energies are in degrees Kelvin per particle.

$\rho\sigma^3$	E_2	$\langle T \rangle$	$\langle V \rangle$
0.328	−6.662 ± 0.035	11.426 ± 0.097	−18.088 ± 0.091
0.365	−6.848 ± 0.018	13.620 ± 0.117	−20.466 ± 0.116
0.401	−6.743 ± 0.033	15.811 ± 0.185	−22.554 ± 0.182
0.438	−6.386 ± 0.072	18.608 ± 0.149	−24.994 ± 0.130
0.490	−5.362 ± 0.079	23.034 ± 0.196	−28.396 ± 0.179

A survey of the computations based on functions of the Jastrow form reveals that it is difficult, if not impossible, to find a form for $f(r)$ which significantly lowers the energy as compared with the energies obtained originally by McMillan and by Schiff and Verlet.[1] This conclusion has recently been reinforced by three calculations[5,22,23] all of which find the best form for $f(r)$ using the Euler-Lagrange equation. Two of these calculations (Refs. 5 and 22) were carried out using the HNC integral equation to compute the energy of the system. Within the latter approximation it is clear that optimizing $f(r)$ lowers the energy by less than 3%. This conclusion was confirmed by an iterative sequence of Monte Carlo variational calculations carried out by Campbell and Pinsky.[23] We thus conclude that the original estimates of the lowest energy of the Lennard-Jones system, namely, −5.95 °K per particle, are unlikely to be lowered by more than 0.2 °K per particle by seeking the best possible Jastrow function. Since the GFMC yields energies −6.85 °K we conclude that the Jastrow form is inadequate as regards computation of the ground-state energy. It is however worth pointing out that changes in the form of $f(r)$ can bring significant improvements in the computed structure function $S(k)$. This was first demonstrated for the Lennard-Jones system by de Michelis and Reatto[4]; similar results have now been established[24] for the hard-sphere system. We will return to this point in Sec. III B. In Fig. 7 we compare our GFMC results, without the three-body potential corrections, with the variational results of Schiff and Verlet.[1]

We now consider the results of the recent calculations which extend the form of the trial function to include explicit three-body correlations. Both calculations yield energies much below the best Jastrow calculations. Campbell and Chang[5] find a lowest energy of −6.58 °K per particle, Pandhuripande[7] finds −6.72 °K per particle. Again, both calculations use approximate integral equations and the results are therefore subject to some uncertainty. Monte Carlo computations based on these new trial functions would be very valuable. The results are so striking that we believe that the inclusion of the correct three-body correlations are likely to bring the variational estimates of the ground-state energy very close to those obtained by our exact method. If this proves to be correct then we can conclude that there are significant three-body correlations in the exact ground state. This conclusion receives support from the variational calculations on the density dependence of the roton spectrum.[25]

We close this section with a general discussion of the accuracy with which variational energies can be computed from Jastrow trial functions. Three exact GFMC studies have been made which are relevant to this discussion; the hard-sphere system,[6] the repulsive Yukawa system[26] and the work reported in this

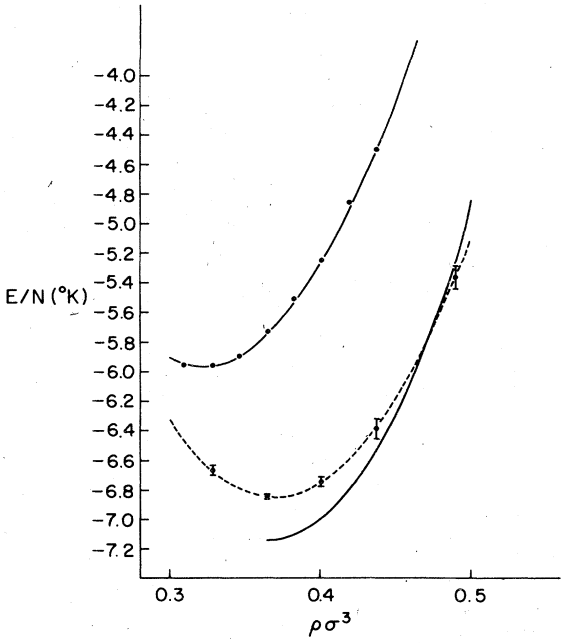

FIG. 7. Comparison of the GFMC and the variational results for the energy. The solid curve represents the experimental data from Ref. 18. The lower dashed curve shows the GFMC results; the upper solid curve gives the variational results using the McMillan trial function.

paper on the Lennard-Jones (LJ) system. In Table VI we show some typical results for these three potentials. The entries E, $\langle T\rangle$, and $\langle V\rangle$ refer to results from the GFMC method. Those labeled with a subscript v refer to variational results based on Jastrow functions and recomputed by Monte Carlo methods. This table shows very clearly that an accurate variational calculation based on a Jastrow function yields kinetic and potential energies which are, for all three potentials, within a few percent of the exact values. For the hard-sphere system the entire energy is kinetic, and consequently the energies E and E_v agree within a few percent. The Yukawa system has a repulsive potential energy and thus the error in the total energy E_v merely reflects the addition of the small errors in $\langle T\rangle_v$ and $\langle V\rangle_v$. However the energy of the Lennard-Jones system is the consequence of a very large cancellation between the kinetic and negative potential energies. It is for the most part this large cancellation that leads to such a large percentage error in the variational energy (21%) as compared with the small errors for the other two potentials. It is interesting to compare the accuracy of the total energy of these systems normalized in a different way. The last column in Table VI contains values of $\Delta E/\langle T\rangle$; where $\Delta E = |E - E_v|$ is the error in the total energy and $\langle T\rangle$ is the expectation value

TABLE VI. Comparison of variational and GFMC calculations.

Potential	E	$\langle T\rangle$	$\langle V\rangle$	E_v	$\langle T\rangle_v$	$\langle V\rangle_v$	$\Delta E/\langle T\rangle$
Hard-Sphere[a]	5.80	5.80	...	6.0	6.0	...	3%
Yukawa[b]	880	180	700	883	160	723	2%
Lennard-Jones[c]	−6.85	13.62	−20.47	−5.68	13.67	−19.35	9%

[a]Hard-sphere data are at a reduced density $\rho a^3 = 0.20$ which is close to the density of the hard-sphere system which is equivalent to the density of liquid helium at zero pressure and $T = 0$. Energies are in units of $\hbar^2/ma^2$.

[b]Yukawa data are at a density of one inverse Fm^3. The quantity $\Delta E/\langle T\rangle$ and the comparisons of $\langle T\rangle_v$ and $\langle V\rangle_v$ with the GFMC estimates are not sensitive to the reduced density. Energies are in MeV per particle.

[c]The Lennard-Jones data are at the equilibrium density $\rho\sigma^3 = 0.365$. Energies are in degrees Kelvin per particle.

of the kinetic energy. Since the kinetic energies are always in good agreement, it does not matter whether we choose to normalize to $\langle T\rangle$ or $\langle T\rangle_v$. We chose this method of normalization because for all three potentials $\langle T\rangle$ is a good measure of a typical energy of the system. We see that this measure of the error in E brings the Lennard-Jones system into somewhat closer agreement with the other potentials.

In summary we believe that variational Jastrow calculations face a special difficulty for the Lennard-Jones system. They yield fairly accurate values for $\langle T\rangle$ and $\langle V\rangle$. The cancellation between these quantities makes an accurate calculation of E very difficult.

B. Pair correlation function and structure function

Figure 8 shows the pair correlation function $g(r)$ obtained by us at the three densities ρ_0, 1.1 ρ_0, and 1.2 ρ_0. These results were all obtained using the McMillan[1] form for the importance function. As discussed in Sec. II D, we also carried out a computation of $g(r)$ at ρ_0 using the Reatto β form[24] for the importance function. The results of this computation were indistinguishable from those obtained with the McMillan form, showing that our method of computation of the pair correlations was insensitive to the importance sampling. We estimate that the errors on any of these curves are less than 1%, except at small values of r where the errors are somewhat larger, about 1.5% at the peak.

Figure 9 compares our results for $g(r)$ at ρ_0 with the experimental data obtained by Achter and Meyer.[27] The experimental curve was obtained by Fourier transforming the $S(k)$ measured at vapor pressure at 1.1 °K. The agreement with experiment is very good and shows that the L-J pair potential is a resonable approximation to the true pair potential as far as reproducing the two-body correlations. It seems likely that three-body potential effects are small. We will not dwell further on more detailed comparisons of theoretical and experimental correlation functions. It is preferable to make a detailed comparison of the structure functions. The structure function can be measured by neutron or x-ray scattering experiments and can be reliably computed theoretically. Such a comparison therefore avoids the difficulties of Fourier transforming limited experi-

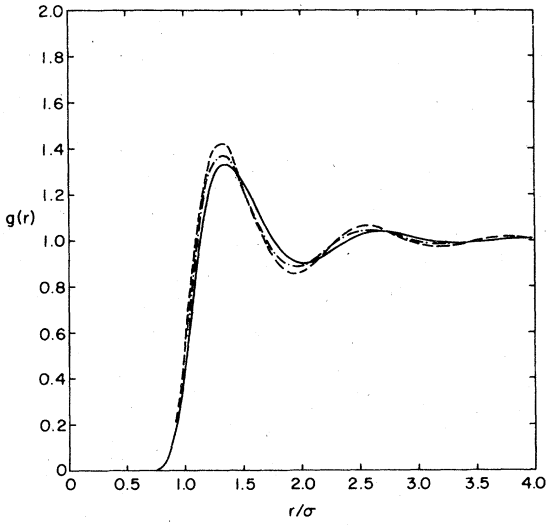

FIG. 8. Radial distribution function $g(r)$ from the GFMC calculation. The solid curve is $g(r)$ at a density $\rho = \rho_0$, where ρ_0 is the equilibrium density of liquid helium at $T = 0$. The dashed and dotted curve is $g(r)$ at $\rho = 1.1\rho_0$, the dashed curve is $g(r)$ at $\rho = 1.2\rho_0$.

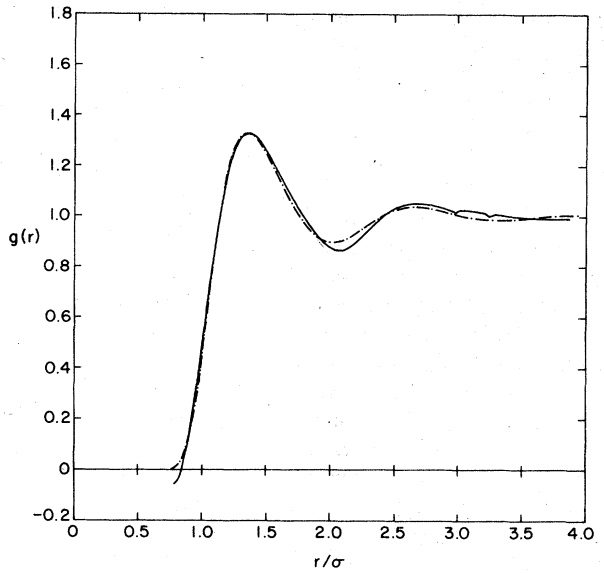

FIG. 9. Comparison of the experimental $g(r)$ with that derived from the GFMC calculation. The solid curve is the experimental data from Ref. 27. The dashed and dotted curve is from the GFMC calculation at the equilibrium density of liquid helium at $T=0$.

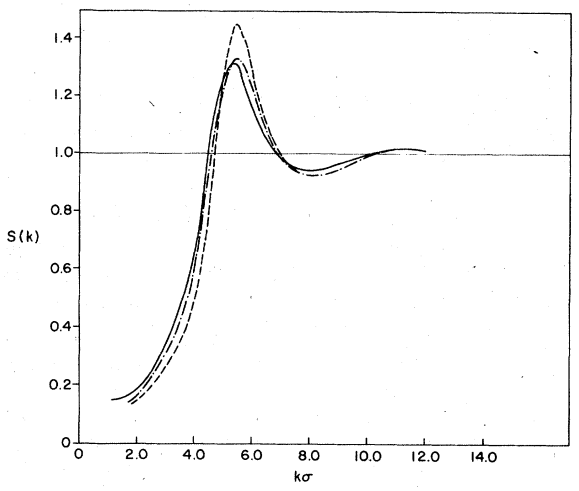

FIG. 10. Liquid structure factor $S(k)$ from the GFMC calculation. The solid curve is at a density ρ_0 equal to the equilibrium density of liquid helium at $T=0$. The dashed and dotted curve is at $1.1\rho_0$ and the dashed curve is at $1.2\rho_0$.

mental data on $S(k)$ to get $g(r)$.

Figure 10 shows our data on $S(k)$ at the three densities ρ_0, 1.1 ρ_0, and 1.2 ρ_0, and Fig. 11 shows our data at ρ_0 compared with the experimental data of Achter and Meyer.[27] These data were taken at 1.1 °K where the density of liquid helium is slightly lower than ρ_0. The density difference is so small that we do not expect that it will significantly affect the comparison. Our data on $S(k)$ was obtained by extending $g(r)$ sufficiently far so that a reliable $S(k)$ could be found by a Fourier transform. The extension technique is described in Appendix C. A direct computation of $S(k)$ is also possible; the results are noisy beyond the first peak and not as reliable as those found by Fourier transforming $g(r)$. As with $g(r)$ the agreement between experiment and theory is very good. The errors in $S(k)$ are estimated to be about 0.02 through the first maximum and decreasing smoothly to 0.01 at the first minimum.

Except at small k we have limited our comparison to the x-ray data of Achter and Meyer for the following reasons. First, these x-ray data seem to us to be more accurate than previous x-ray data. They are in good agreement with the earlier results of Gordon, Daunt, and Shaw.[28] Second the neutron data that is available is confusing. Recent data by Cowley and Woods[29] is in fair agreement with older work by Hurst and Henshaw,[30] and both sets of data agree well with the Achter and Meyer data. The often quoted data of Henshaw[31] does not agree with the other neutron data or with the x-ray data. This discrepancy has received no explanation.[29]

Caution should be exercised in making detailed comparisons of the GFMC structure factor computed from the Lennard-Jones potential with the experimental $S(k)$. We have seen in Sec. III A that the Lennard-Jones potential does not adequately represent the two-body interactions in liquid helium. It may therefore produce errors in $S(k)$ which will mislead one in any very precise comparison with experiment. Recent variational work[5,32] suggests that $S(k)$ may change somewhat when a more realistic two-body potential is used.

In Fig. 12 we compare our small k data with the experimental data due to Hallock.[33] Our data were generated by the method described in Appendix B. It should be pointed out that since the GFMC method is exact our calculations for a finite system must contain some of the effects of the correlations due to the zero-point motions of the phonons. From Fig. 12 we see that our data fall systematically below the experimental data in the range, although the two curves are nowhere more than two standard errors apart. If the discrepancy is real it must again be a consequence of using the Lennard-Jones potential. Unfortunately there are no low-temperature data at higher densities that might be compared with our numerical results at 1.1 ρ_0 and 1.2 ρ_0.

We now turn to a comparison of our results with other theoretical computations. First we make a comparison with the exact GFMC results on hard spheres obtained by KLV. This comparison is made to understand how well the pair correlations in the Lennard-Jones system can be modeled by those of the hard-sphere system. After this comparison we turn to several of the variational computations that have been made in the last decade. Our aim here is to try to understand how accurately the various trial functions can reproduce the local structure in the fluid.

In order to make a comparison with the hard-sphere system we have to decide on a method of choosing the reduced density ($\rho' a^3$) of the hard-sphere system. Here ρ' is the number density of the hard-sphere system and a is the hard-core diameter. This question was discussed at some length by KLV who give convincing arguments. One argues that the repulsive part of the shifted Lennard-Jones potential plays the role of a hard core. Then we characterize this term by its S-wave scattering length l. This then leads to the statement that in order for the hard-sphere system to represent the Lennard-Jones system we should choose ρ' so that $\rho' a^3 = \rho l^3$, where ρ is the density of the Lennard-Jones system. This equation then yields the result that $\rho' a^3 = 0.2318$ when ρ is equal to the equilibrium density of the L-J system. As we have seen in Sec. III A this equilibrium density is very close to that found experimentally for liquid helium. Figure 13 shows the comparison obtained by this method. The agreement is generally good, although there are clearly small discrepancies.

Of course one could turn the scaling argument around and ask the question can we find any reduced density ($\rho' a^3$) for which the hard-sphere correlation function is in good agreement with that of the L-J system. Figure 13 clearly shows that this can be done. One then asks how to scale lengths from one system to another and finds that the required length is $l^3 = \rho' a^3/\rho$ which is numerically equal to the S-wave scattering length for the repulsive part of the Lennard-Jones potential.

We find this comparison illuminating. It tells us that the quantum Lennard-Jones two-body correlations can be modeled by hard spheres in a very similar way to the well-known classical modeling of the LJ system by classical hard spheres. It also supports our contention in Sec. III A that the hard-sphere system can be used as a reference system to compute the thermodynamic properties of the Lennard-Jones system.

We turn now to a comparison with variational calculations. The early variational calculations of $S(k)$ by McMillan[1] and Schiff and Verlet[1] are in good agreement with each other. Figure 14 shows our data compared with theirs. Generally our data shows significantly more structure, our first peak being higher

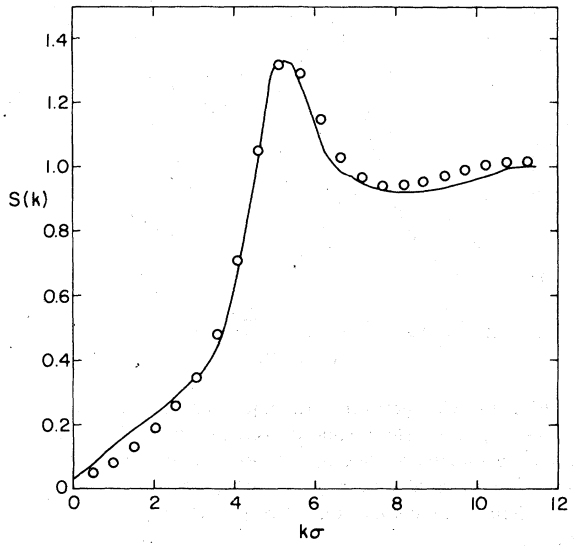

FIG. 11. Comparison of the experimental liquid structure factor $S(k)$ with that derived from the GFMC calculation. The solid curve is the experimental data from Ref. 27. The circles are the data from the GFMC calculation at the equilibrium density of liquid helium at $T=0$.

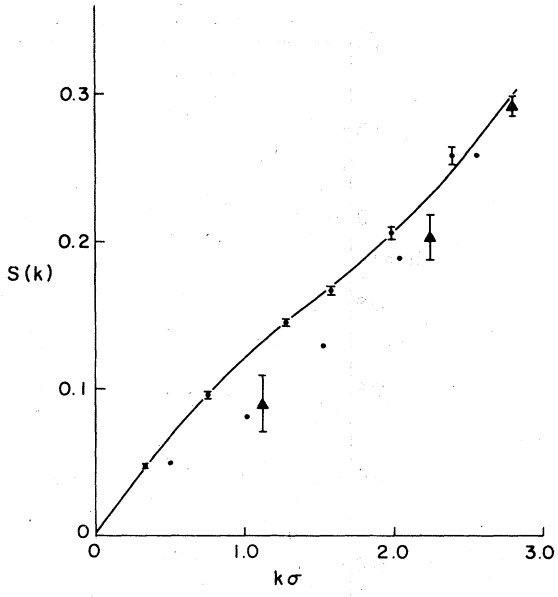

FIG. 12. Comparison of the experimental liquid structure factor at small wave numbers with that derived from the GFMC calculation. The solid curve passing through the points with error bars is the experimental data from Ref. 33. The dots are the results from the GFMC calculation; typical error bars for these results are shown for three points with triangles.

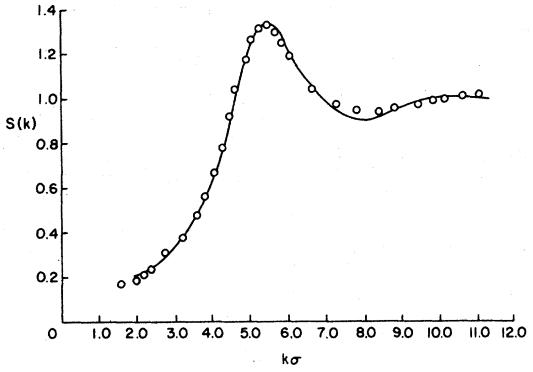

FIG. 13. Comparison of the liquid structure factor for the hard-sphere system, solid curve, and the Lennard-Jones system, open circles. The comparison is made using the data from the hard-sphere system at the reduced density equivalent to the equilibrium density of the Lennard-Jones system.

and our first minimum lower. This result has been noted in other comparisons of the same kind.[6,26] In addition our first peak occurs at a smaller value of k. It has been a long standing defect of the early variational work that the first peak always occurred at too large a value of k. Our results now show that this is almost certainly a defect of the variational wave function and not the two-body potential.

Recently several attempts have been made to improve the form of the trial function in the variational calculations. As we remarked in Sec. III A two approaches can be distinguished, either one tries to improve the two-body correlations in the traditional Jastrow form of trial function or one adds explicit three-body correlations[5,7] to the trial function. The first approach has been taken by McGee and Murphy,[34] Reatto,[4,24] Lantto *et al.*,[22] and Chang and Campbell.[5] A detailed discussion of this work would take us far from our main objective. We believe it can be well summarized as follows. It is possible to change the two-body correlations in the trial function so that $S(k)$ is in better agreement with experiment. In particular Reatto's very detailed study of this question yields convincing results. However the variational energy was not improved, and in some cases was raised, by the new trial functions used by de Michelis and Reatto. Chang and Campbell[5] and Lantto *et al.*[22] both attempt to optimize the Jastrow two-body correlations by different approximate methods. Both obtain, as we have noted in Sec. III A, somewhat improved energies. Chang and Campbell also obtain an improved structure function although there are still discrepancies as compared with experiment. However it is very difficult to assess this work rigorously as approximations of un-

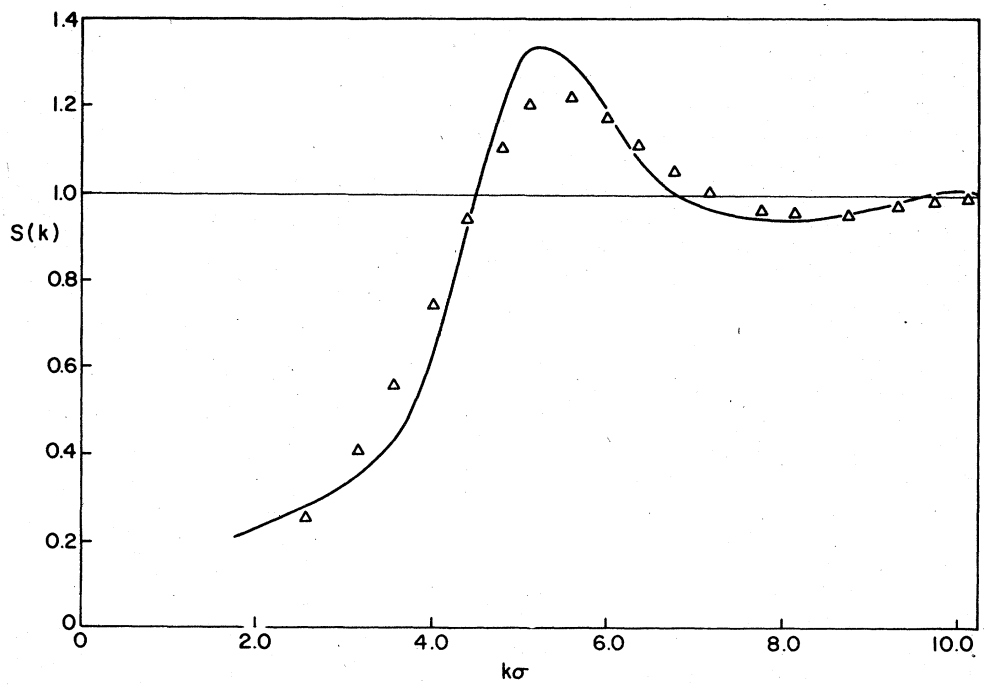

FIG. 14. Comparison of the liquid structure factor $S(k)$ from the GFMC calculation (solid line) with that obtained from a variational calculation using the McMillan form for the trial function. The latter results are represented by the open triangles. Both curves are at the equilibrium density of liquid helium at $T=0$.

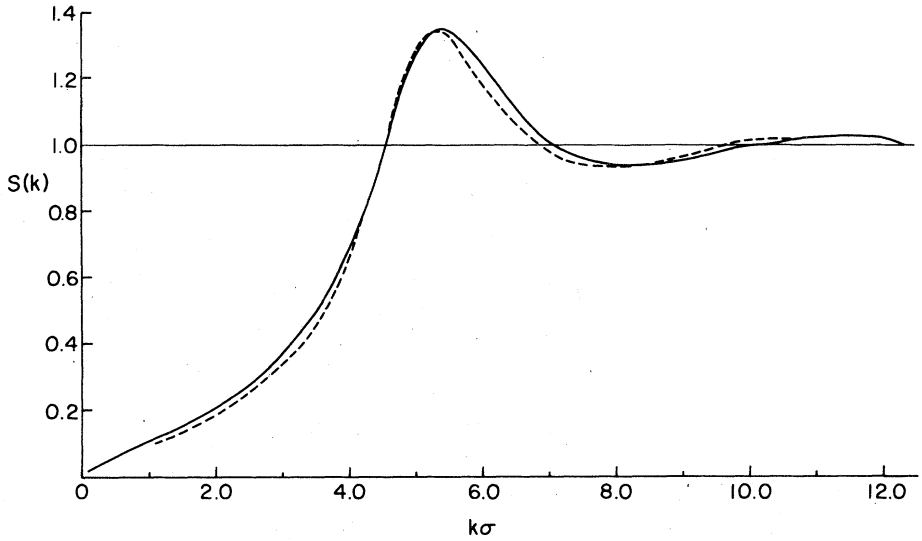

FIG. 15. Comparison of the liquid structure factor derived from the GFMC calculation (solid line) with that calculated variationally (dashed line) by Campbell and Chang (Ref. 5). Both sets of results are for liquid helium at its equilibrium density at $T=0$.

known validity were used in computing the structure function.

Chang and Campbell[5] and Pandharipande[7] have both introduced explicit three-body correlations into the variational function. As we have noted in Sec. III A both find significantly lower energies. Pandharipande has not published a structure function. His $g(r)$ has too little structure as compared with the experimental $g(r)$. Chang and Campbell's $S(k)$ is in much better agreement with experiments than those derived from variational functions using only two-body correlations. We compare the structure function computed by Chang and Campbell with our own in Fig. 15. It is in good agreement with ours. This work suggests that three-body correlations are important and should be included in the trial functions. However since both calculations depend on approximate methods no definite conclusions can be made at this time. One needs a Monte Carlo estimate of the effects of three-body correlations on $S(k)$ and on the energy.

In Appendix D we present tables (see Tables XIV–XVII) of both $g(r)$ and $S(k)$ at several densities.

C. Single-particle density matrix and momentum distribution

In this section we present our results for the single-particle density matrix $\rho_1(r)$ and its Fourier transform, the momentum distribution $n(k)$.

Figure 16 shows our results for $\rho_1(r)$ at the three densities ρ_0, 1.1 ρ_0, and 1.2 ρ_0. Each set of data was obtained using the McMillan importance function and then extrapolated as described in Sec. II. These graphs clearly show that $\rho_1(r)$ is quite strongly dependent on the density. The asymptotic value reached at large r is equal to the fraction of particles with zero momentum, n_0.[17] We shall discuss this quantity in more detail in the next paragraph. The small amount of structure in these curves at large values of r is within the range of our computational

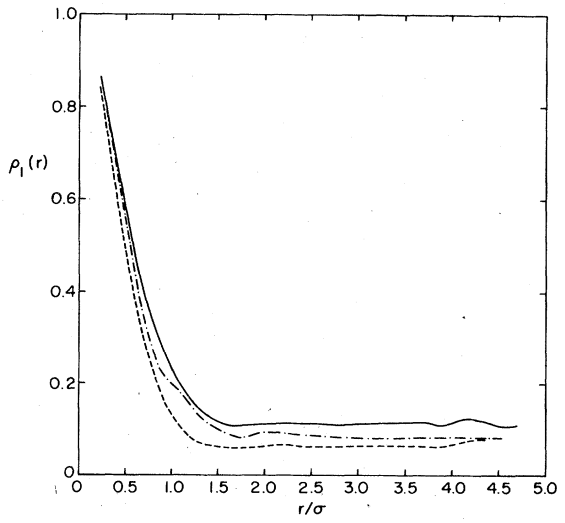

FIG. 16. Single-particle density matrix $\rho_1(r)$ derived from the GFMC calculations. The solid curve is $\rho_1(r)$ at the equilibrium density (ρ_0) of liquid helium at $T=0$. The dashed and dotted curve is at $1.1\rho_0$ while the dashed curve is at $1.2\rho_0$.

TABLE VII. Fraction of particles (n_0) in the zero-momentum state as a function of density. The first column gives the density in reduced units.

$\rho\sigma^3$	n_0
0.365	0.113 ± 0.002
0.401	0.085 ± 0.002
0.438	0.062 ± 0.002
0.490	0.035 ± 0.001

errors and should not be taken as real. Table VII shows our results for n_0 for several densities. It can be seen that it is an approximately linear function of the density, becoming small near the freezing density ($\rho = 0.473\sigma^{-3}$).

At the equilibrium density ρ_0 we have also computed n_0 using the Reatto β function for importance sampling. The results (Table II) are identical within our errors.

The basic difficulty in extracting n_0 from $\rho_1(r)$ is that one needs to know $\rho_1(r)$ for as large values of r as possible. Since our computations are limited to fairly small systems (64 and 128 particles) we cannot claim to have rigorously established the asymptotic limit of $\rho_1(r)$. Clearly, computations on much larger systems would be desirable. However even with our small systems we detect little change in n_0 as we double the number of particles from 64 to 128. Apart from the size dependence and fluctuations at the largest values of r, the curves of $\rho_1(r)$ do not have large statistical variation. We estimate our error in n_0 to be 5% at ρ_0 and 10% at other densities.

There have been several attampts[29,35–40] to extract n_0 from neutron scattering measurements. That this might be possible was first suggested by Hohenberg and Platzman.[41] An excellent review of the difficulties inherent in obtaining n_0 from the scattering data has been given by Cowley.[42] We find that the most convincing analysis is due to Woods and Sears.[43] There are still uncertainties in the results due in part to insufficient data and to the fact that the lowest temperature at which data were taken is 1.1 °K. We do not regard this latter point as being a serious impediment in making a comparison with our ground-state data. At 1.1 °K, liquid helium is still very cold, with few thermal excitations. It seems plausible that n_0 will have changed little from its ground-state value, but this qualitative argument should be checked by measurements at much lower temperatures.

Woods and Sears[43] find a value of 0.069 for n_0 at 1.1 °K. The error quoted is ±0.008. Taken at its face values this result contradicts our own value of 0.12. However, as we have just pointed out, the amount of data available places serious limitations on how accurately n_0 is known. We await the analysis of new experiments and would encourage experimentalists to undertake experiments at more than one density and at as low a temperature as possible. Other experimental data and subsequent analysis[36,38–40] have yielded values for n_0 substantially lower than that due to Woods and Sears. We do not find the data analysis on which these results depend to be as convincing as that due to Woods and Sears.

We turn now to the remainder of the momentum distribution; $n(k)$ ($k \neq 0$). Our results for this are plotted as $kn(k)$ in Fig. 17. Clearly there is a strong density dependence in $n(k)$. In Sec. II D, we commented that the change in $n(k)$ as calculated from different importance functions is less than the errors which are of the order of 10%. $n(k)$ is more difficult to compute than $S(k)$ and longer runs will be needed to obtain more accurate results. Fortunately the errors in $n(k)$ are not so large as to prevent us from making several interesting observations and comparisons.

The structure at large k is within the statistical errors of our calculations but that at intermediate k is significant. We believe that our data suggests that there may be a small minimum in $kn(k)$ at intermediate k. A comparison of Fig. 17 with Fig. 2 shows that the density dependence is also much larger than the changes in $n(k)$ due to the importance function. Indeed $n(k)$ is strongly dependent on ρ, much more so than $S(k)$. The physics behind this eludes us but is worth further invesigation.

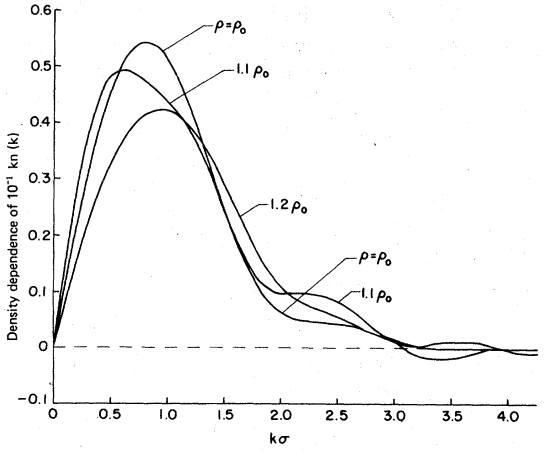

FIG. 17. Momentum distribution $n(k)$ derived from the GFMC calculation. The equilibrium density of liquid helium at $T = 0$ is ρ_0. The fluctuations in the curves at large k are not statistically significant.

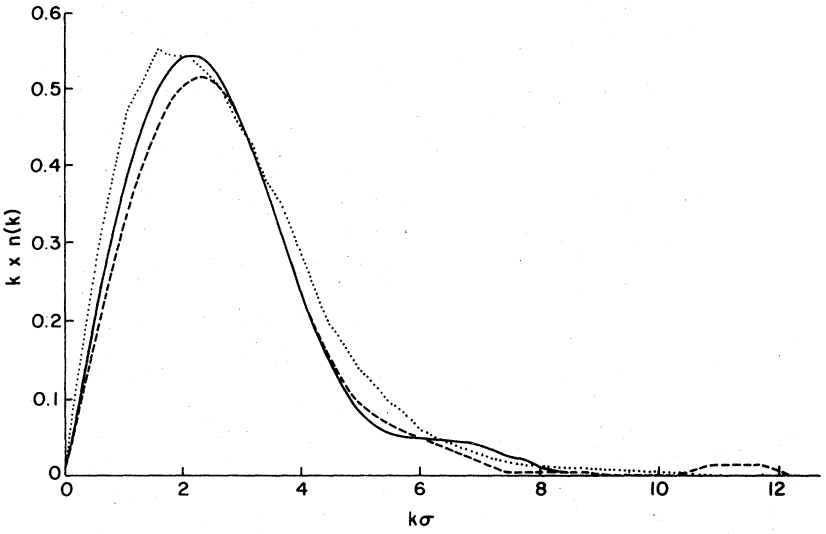

FIG. 18. Comparison of the momentum distribution $n(k)$ derived from the GFMC calculation with the experimental results from Ref. 43. The two GFMC curves are the solid curve based on the McMillan importance function and the dashed curve based on the Reatto β importance function. The experimental data are given by the dotted curve.

We now compare our data for $n(k)$ at ρ_0 with the experimental values due to Woods and Sears[43] in Fig. 18. The experimental curve is obtained by analyzing neutron scattering data.

The general shape of the curve is semiquantitatively established by these data. Our own results are in agreement, within the rather large experimental uncertainties. Again we do not believe that the elevated temperature of 1.1 °K seriously affects the comparison. Another comparison should however be made. The strong theoretical density dependence should be looked for experimentally. At this stage it may be more interesting to compare trends in $n(k)$ with density rather than emphasizing a comparison at a single density. Again data at a much lower temperature would be desirable.

A more limited yet more refined comparison can be made. The mean kinetic energy $\langle T\rangle$ of the system is proportional to the second moment of $n(k)$. Woods and Sears[20] have shown how an estimate of $\langle T\rangle$ can be extracted from the moments of the neutron scattering cross section. Their analysis is convincing and internally self-consistent in that several different moments give almost the same value for $\langle T\rangle$. They find a value of 13.5 °K ±1.2 °K at 1.1 °K for $\langle T\rangle$. Our own values (from Table V) give a value of 13.62 ±0.12. These are values obtained from $\langle T\rangle = E - \langle V\rangle$, where E is exact and $\langle V\rangle$ is extrapolated, and yield values independent of the importance function. The agreement is excellent, although we wish for smaller experimental errors. Overall we find the agreement of our momentum distribution with experiment encouraging. We will certainly attempt to improve our results and we hope that the experimentalists will also be able to improve theirs.

A comparison of $n(k)$ and n_0 for the Lennard-Jones system with that for the hard-sphere system is revealing. KLV obtained a value of n_0 of 0.117, at a density 5% less than the density equivalent to the equilibrium density of liquid helium. This value is lower than ours of 0.12 at the equilibrium density, but the discrepancy is inside the range of the computational error of the KLV result.

In Fig. 19 we compare our GFMC results for the

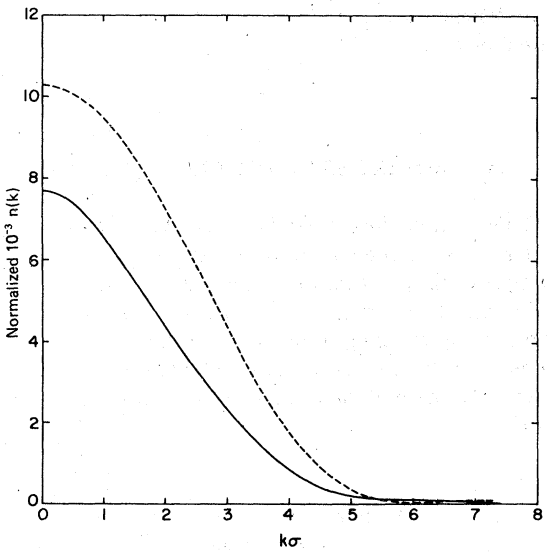

FIG. 19. Comparison of the momentum distribution of the Lennard-Jones fluid, the solid curve, with the hard-sphere fluid, the dashed curve. Both results were obtained by the GFMC method and both are normalized so that the three-dimensional integral of $n(k)$ is equal to $1 - n_0$, where n_0 is the fraction of particles with zero momentum.

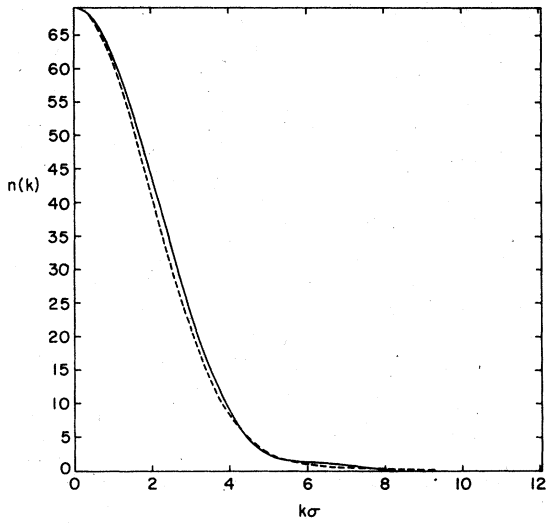

FIG. 20. Comparison of the momentum distribution $n(k)$ derived from the GFMC calculation with the distribution derived from a variational calculation using the McMillan trial function. Both sets of data are for the equilibrium density of liquid helium at $T=0$.

Lennard-Jones system with the GFMC results for the hard-sphere system. The comparison is made at the equivalent hard-sphere reduced density and both curves are normalized so that the three-dimensional integral of $n(k)$ is $1-n_0$.

The final comparison we make is between the GFMC results and the variational results. This is shown in Fig. 20 which reveals that the two momentum distributions are identical within our computational errors.

IV. PROPERTIES OF THE CRYSTAL PHASE

This section closely parallels Sec. III. We present our results for the equation of state, pressure, compressibility, structure factor, and momentum distribution of the crystal phase. In addition we discuss the melting-freezing transition and the single-particle density. Wherever possible we compare our results with experimental data and with previous variational work.

A. Equation of state of the crystal phase

We have computed the energy of the fcc crystal in the density range $\rho\sigma^3=0.420$ to $\rho\sigma^3=0.589$. We chose to limit our computations to the fcc phase because it was technically convenient and because previous variational and GFMC calculations had been performed for that phase. In addition the variational work of Hansen[44] had shown that the differences between the equation of state of fcc and hcp are small. We repeated his calculations in the course of the present study, improving the statistics and decreasing the possible difference in energy between these two phases. Of course the determination of the freezing-melting transition is rather sensitive to the equations of state. We enlarge on this point in Sec. IV B. At densities less than $\rho\sigma^3=0.512$ the fluid phase has a lower energy and our results refer to metastable crystal states. We can thereby determine the densities at which melting and freezing take place (Sec. IV B) and to make a number of interesting comparisons with previous variational work. We have not extended our results to the higher density range covered variationally by Hansen and Pollock.[45]

A few words of explanation are necessary to explain how in the GFMC method one distinguishes between a crystal and a fluid. This distinction is made in practice by the choice of the importance function (see Sec. II D). For a fluid phase calculation we always use a function which is translationally invariant, for example a Jastrow function with the parameters determined variationally. If we wish to compute the properties of a crystal phase then we choose the importance function so that it localizes the particles on the lattice sites for a chosen crystal symmetry. In a stable region of the crystal phase we find that for a very long GFMC computation that the particles remain localized in the neighborhood of the original lattice sites. These importance functions we have used are not symmetric. We are therefore simulating Boltzman rather than Bose crystals. For particles interacting with a stiff core potential, such as the Lennard-Jones potential, exchange is exceedingly rare in the solid phase.[12]

As was explained in Sec. II D, localization on lattice sites is not necessary in principle. The technique is merely used as a device to speed the convergence of the iterative GFMC procedure. In Sec. II D we showed that at one particular density ($\rho\sigma^3=0.526$) the physical properties we compute using this biasing procedure are independent of the parameters in the importance function. The localization parameter [A in Eq. (2.16)] was changed by 20%. The results of the GFMC calculation were unchanged within our fairly small errors.

Our computations were again carried out with the standard Lennard-Jones potential and perturbation estimates of the three-body potential term V_3, Eq. (A1), added to our GFMC results. When tail corrections were added there was no difference, within our errors, between the results for a 32 and 108 particle system. We estimate (see Sec. II C) that the errors in the eigenvalues are less than 1%. The error in the perturbation estimate of $\langle V_3\rangle$ is less than 2% of the

additional energy. The correction to the energy due to the long-range correlations introduced by the zero-point motion of the compressional phonon modes again turned out to be completely negligible.

Table VIII contains our results for the crystal phase. As in the fluid phase, we have fitted our results to a polynomial of the form

$$\frac{E}{N} = A' + B'\left(\frac{\rho-\rho_1}{\rho_1}\right)^2 + C'\left(\frac{\rho-\rho_1}{\rho_1}\right)^3 . \qquad (4.1)$$

The values of the parameters are

$$A' = 5.46 \pm 0.17, \quad B' = 14.08 \pm 27 ,$$

$$C' = 9.02 \pm 22 ,$$

and

$$\rho_1 = (0.416 \pm 0.072)\sigma^{-3} .$$

The values of A', B', and C' are given in degrees Kelvin. It can be seen from Fig. 21 that this form gives an excellent fit to our data. The errors in the parameters appear to be very large; however it must be emphasized that the errors are highly correlated, a fact taken into account when computing the pressure and compressibility. Results for the equation of state are compared with the experimental data of Edwards and Pandorf[46] in Fig. 21.

From Table VIII we see that at the lowest density where the crystal is stable the difference between our theoretical results (−5.22 °K) and the experimental results (−5.96 °K) is about 0.7 °K per particle. This is very similar, though somewhat larger, than the almost constant discrepancy we found in the fluid phase (0.5 °K per particle). However as the density increases in the crystal phase the discrepancy decreases rather quickly, reaching a value of 0.2 °K per particle at the highest density. This is to be contrasted with the fluid phase where the density dependence of our theoretical results was very similar to that of the experimental data. We conclude that at the higher densities of the crystal phase the Lennard-Jones potential is much less adequate than in the fluid phase.[47]

From Table VIII it is clear that the balance between $\langle T\rangle$ and $\langle V\rangle$ becomes more and more delicate as the density increases. At our highest density the total binding energy (−2 °K) is only 7% of $\langle T\rangle$ or $\langle V\rangle$. Thus it is not very helpful to express the difference between our computed energies and the experimental energies as a percentage. At a slightly higher density the binding energy will go through zero and any discrepancy will then be infinite. It would be illuminating to have experimental information values for $\langle T\rangle$ and/or $\langle V\rangle$. Unfortunately this type of information is exceedingly difficult to extract from experimental data. There is however hope that $\langle T\rangle$ can be extracted.[20] It would be interesting to have measurements of this quantity in the crystal phase.

We should also comment on our use of perturbation theory to estimate $\langle V_3\rangle$. As we have just mentioned the ground-state energy computed from the unperturbed Hamiltonian becomes small at the highest density and will become even smaller at higher densities. On the other hand, our perturbation estimates of $\langle V_3\rangle$ suggest that this quantity will steadily increase. There will then be a range of densities for which $\langle V_3\rangle$ is comparable with the ground-state energy. It might be thought that in this range of densities, perturbation theory has broken down. We think that this conclusion is not correct. A better comparison is between $\langle V_3\rangle$ and $\langle V\rangle$ or $\langle T\rangle$; either of these quantities is a typical energy of the system. Such a comparison shows that $\langle V_3\rangle$ is about 1.5% or $\langle T\rangle$ or $\langle V\rangle$ at the highest density.

Because our energies have the wrong density

TABLE VIII. Energy of the crystal phase calculated with the GFMC method. The first column gives the density in reduced units, E_2 is the energy computed using the Lennard-Jones potential, $\langle V_3\rangle$ is the perturbation estimate of V_3, $E = E_2 + \langle V_3\rangle$, and E_{exp} is the experimental value of the energy taken from Ref. 46. All energies are in degrees Kelvin per particle.

$\rho\sigma^3$	E_2	$\langle V_3\rangle$	E	E_{exp}
0.420	−5.671 ± 0.059	0.227 ± 0.004	−5.444 ± 0.059	...
0.440	−5.679 ± 0.050	0.253 ± 0.003	−5.426 ± 0.050	...
0.468	−5.503 ± 0.053	0.301 ± 0.002	−5.202 ± 0.053	−6.06 ± 0.05
0.526	−4.718 ± 0.032	0.413 ± 0.002	−4.305 ± 0.032	−5.03 ± 0.05
0.589	−2.929 ± 0.092	0.562 ± 0.003	−2.367 ± 0.092	−2.70 ± 0.05

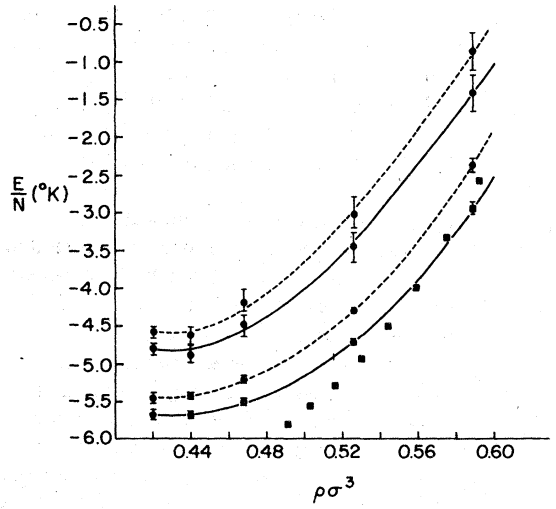

FIG. 21. The energy of the crystal phase. The experimental energies from Ref. 46 are shown as solid squares (■). The lowest solid curve represents the GFMC results without the addition of the perturbative estimate of V_3. The lower dashed curve includes the estimate of V_3. The upper solid and upper dashed curves represent the variational results without and with the estimate of V_3, respectively.

dependence our pressures in the crystal phase are in somewhat poorer agreement with experiment than those of the fluid phase. This is clearly shown in Table IX. The computed and experimental values for the compressibility are in fair agreement. Figures 22 and 23 show these results graphically.

In summary, we believe that our GFMC results show that the Lennard-Jones potential is becoming seriously inadequate in the crystal phase. This suggests strongly that future work to test two-body potentials should cover a density range that encompasses both fluid and crystal phases. The detailed comparison of energies depends upon $\langle V_3 \rangle$ which has become a significant part of the crystal energy. It would be well to have independent evidence of the validity of the Axilrod-Teller three-body potential.

We again attempted to test the consistency of our numerical techniques by computing both the virial and thermodynamic pressures in the crystal phase. Exactly the same difficulties arose as we found in the fluid phase (see Sec. III A), and no useful comparison was possible between the two pressures.

In KLV perturbation estimates were made of the energy of the crystal phase. These estimates were subject to rather large errors. Within these errors the perturbation estimates agree with our own values. Note that we are comparing our energy values without any corrections due to V_3. As in the fluid phase this suggests that one can make a successful perturbation theory of ^{4}He using hard spheres as a reference system. A more detailed exploration of this idea would be well worthwhile.

We turn now to a comparison of our GFMC results with the variational results obtained by Hansen[44,48] Table X shows this comparison. The GFMC results are lower in energy by about 1 °K. Again we must remark on the delicate cancellation that is taking place between $\langle T \rangle$ and $\langle V \rangle$. It is extremely easy to be 1 °K off in the total energy when both these quantities are about 35 °K in magnitude; 1 °K is only 3% of either. Indeed a comparison of the variational potential and kinetic energies with those obtained by the GFMC method shows discrepancies ranging from 2–6%. The comparison we made in the fluid phase where we computed $\Delta E/\langle T \rangle$ is also interesting for the crystal phase. Here ΔE is the difference between the variational energy and the GFMC energy, and $\langle T \rangle$ is the expectation of the kinetic energy calculated by either method. The last column in Table X

TABLE IX. Comparison of the pressure and compressibility with experimental data. The first column gives the density in reduced units, p is in atmospheres, and κ is inverse atmospheres. The experimental data are from Ref. 46.

$\rho\sigma^3$	p	p_{exp}	$10^2\kappa$	$10^2\kappa_{exp}$
0.491	28.182 ± 1.9	31.8	0.373 ± 0.038	0.334
0.503	35.115 ± 2.2	41.1	0.326 ± 0.024	0.288
0.516	43.534 ± 2.4	51.8	0.283 ± 0.020	0.246
0.530	53.729 ± 2.5	63.3	0.244 ± 0.024	0.209
0.544	65.180 ± 2.7	77.4	0.212 ± 0.029	0.178
0.559	78.941 ± 3.9	95.2	0.184 ± 0.032	0.148
0.575	95.445 ± 6.5	116.2	0.159 ± 0.034	0.129
0.592	115.201 ± 10.8	140.7	0.137 ± 0.035	0.116

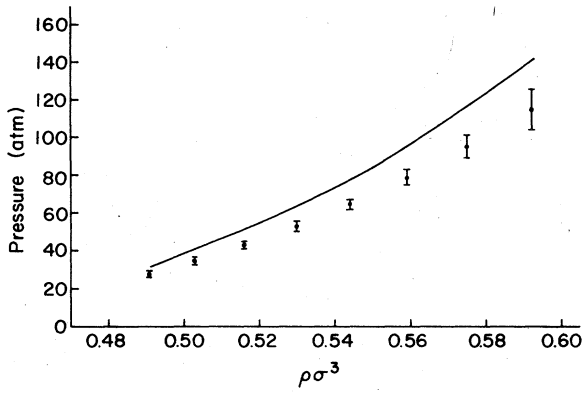

FIG. 22. Comparison of the experimental values for the pressure of the crystal phase (Ref. 46) with the results from the GFMC calculations. The calculated results are shown as points with error bars.

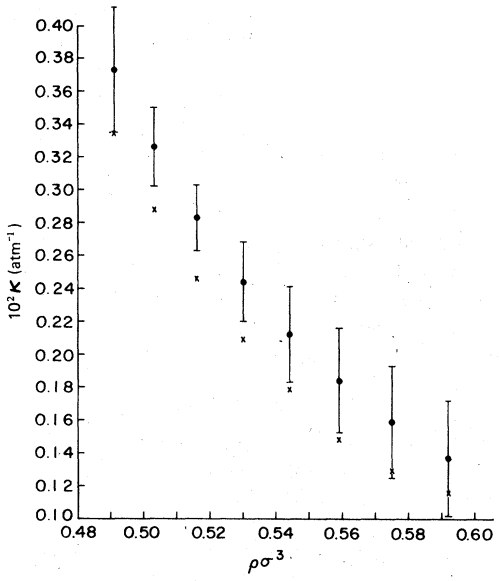

FIG. 23. Comparison of the experimental data for the compressibility of the crystal phase (Ref. 46) with the results from the GFMC calculation. The calculated results are shown as points with error bars and the experimental data are shown as crosses.

shows that this ratio is consistently in the range of 4–5%. This is very similar to the value found in the fluid phase and in other systems.[26] It is worth noting that Fig. 21 shows that the density dependence of the variational results is very similar to that of the GFMC results. The two curves are merely shifted by approximately 1 °K. Clearly both methods of calculation are in need of a better two-body potential.

We suspect that the major source of this discrepancy between the variational results and our own is that the trial functions contained no explicit three-body correlations. It would be interesting to extend the recent variational work on trial functions with three-body correlations from the fluid to the crystal phase.

B. Melting-freezing transition

The equations of state we have established in the fluid and crystal phases allow us to determine the densities at which freezing and melting occur in our model system. This is done in the usual manner using the Maxwell double tangent construction. We determine the slope of the tangent by differentiating the forms, Eqs. (3.1) and (4.1), that have been fitted to our data. The resulting algebraic equation was solved numerically to determine the transition densities. Figure 24 shows this construction and Table XI shows our results for the freezing and melting densities together with the experimental values. The variational results are those quoted in Hansen and Pollock.[45] Before discussing these results we must remind the reader that we have computed the energy of fcc solid helium, whereas the phase transformation which takes place at absolute zero is to an hcp phase.

TABLE X. Comparison of exact and variational energies for the crystal phase. The first column gives the density in reduced units. E_2, $\langle V\rangle$, and $\langle T\rangle$ are the total, potential, and kinetic energies computed by the GFMC method using the Lennard-Jones potential. $(E_2)_v$, $\langle V\rangle_v$, and $\langle T\rangle_v$ are the same quantities calculated using the variational method. The last column gives $\Delta E = |E_2 - (E_2)_v|$ as a percentage of $\langle T\rangle_v$. All energies are in degrees Kelvin per particle.

$\rho\sigma^3$	E_2	$\langle V\rangle$	$\langle T\rangle$	$(E_2)_v$	$\langle V\rangle_v$	$\langle T\rangle_v$	$\Delta E/T$
0.420	−5.671	−24.404 ± 0.095	18.733 ± 0.112	−4.780 ± 0.072	−24.385 ± 0.064	19.605 ± 0.096	4.5%
0.440	−5.679	−25.756 ± 0.096	20.077 ± 0.108	−4.697 ± 0.062	−25.375 ± 0.046	20.678 ± 0.077	4.7%
0.468	−5.503	−27.765 ± 0.073	22.262 ± 0.090	−4.505 ± 0.041	−26.082 ± 0.037	21.575 ± 0.055	4.6%
0.526	−4.718	−31.873 ± 0.099	27.155 ± 0.104	−3.499 ± 0.091	−29.561 ± 0.072	26.062 ± 0.116	4.7%
0.589	−2.929	−35.902 ± 0.147	32.973 ± 0.173	−1.294 ± 0.064	−31.605 ± 0.053	30.311 ± 0.083	5.4%

In other words, our results are valid for the hypothetical liquid - fcc crystal transition rather than for the actual liquid - hcp transition. As we remarked in Sec. IV A possible small differences in the energies (0.1 °K per particle about equal to the errors in the variational calculations), of the two crystal phases may be important in determining the parameters of the transition. A more accurate determination of the transition must await more accurate variational and GFMC computations on the hcp phase. We expect to complete such work in the near future.

Our melting and freezing densities are about 10% higher than the experimental values. Because of this, the theoretical melting pressure is very much higher than the experimental value. On the other hand, the volume change between the phases is 1.6 cm^3/mole which is rather close to the experimental value of 1.9 cm^3/mole. The location of this transition is a severe test of any theory. The discrepancies we find are either due to the inadequacies of the Lennard-Jones potential or to the fcc phase being used rather than the hcp. It is worth commenting that the addition of the perturbation estimates of $\langle V_3 \rangle$ makes a negligible change in the freezing and melting densities.

An important comparison is between the freezing and melting of the Lennard-Jones system and the hard-sphere system. It is now fairly well established that the classical Lennard-Jones transition is very closely related to the freezing of the classical hard-sphere system. This establishes that the classical transition is a packing phenomenon. KLV and Hansen and Pollock have both suggested that the same may be true for the quantum-mechanical Lennard-Jones system. We make the comparison as follows. In Sec. III B we discussed how one could scale the quantum hard-sphere system so that it can be comparted with the Lennard-Jones system. This lead to the statement that the equilibrium density ρ_0 of liquid helium corresponds to a reduced hard-sphere density, such that $\rho a^3 = 0.2138$, where a is the hard-sphere diameter. Our freezing and melting densities

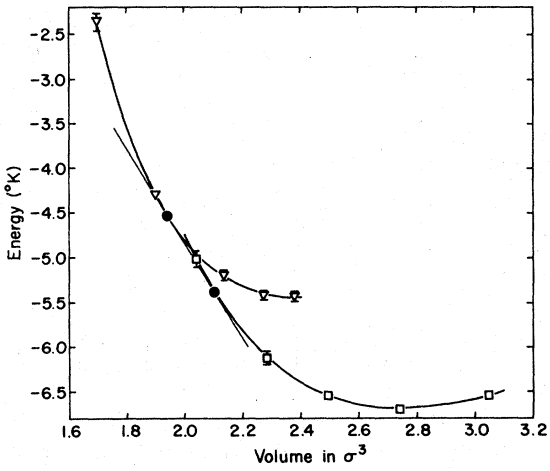

FIG. 24. Double tangent construction which locates the freezing and melting volumes. The upper curve is for the crystal phase, the lower for the fluid phase. The two points of common slope are shown as solid circles (●).

correspond to 1.29 ρ_0 and 1.40 ρ_0, respectively. This implies that if the pure-hard-sphere transition exactly represents the Lennard-Jones transition then its freezing and melting densities should be given by $\rho a^3 = 0.276$ and $\rho a^3 = 0.30$. The actual transition densities, ($\rho a^3 = 0.23$ and 0.25, respectively) found are in fair agreement with these.

In KLV perturbation, corrections were made to include the effect of the attractive part of the potential. The resulting energies contain rather large uncertainties. Within these uncertainties the transition densities agree with our own. Therefore it appears that while the major cause of the transition is a quantum hard-sphere packing phenomenon, the attractive part of the potential reduces the density at which it takes place.

Examination of Table XI shows that the best variational estimates for the transition densities are lower

TABLE XI. Melting-freezing transition. The first column gives the potential and method used. The next two columns give the freezing and melting densities in reduced units. Column four gives the transition pressure in atmospheres. The last column gives the volume difference between the solid and liquid in cubic centimeters per mole. We find no difference in the melting and freezing densities, transition pressure and volume difference if we omit the corrections due to $\langle V_3 \rangle$.

Potential	$\rho_l \sigma^3$	$\rho_s \sigma^3$	p (atm)	ΔV (cm^3/mole)
$V_2 + V_3$	0.475 ± 0.011	0.515 ± 0.009	42.85 ± 8.64	1.63
V_2 variational	0.380	0.457	15.0	4.5
Experiment	0.430	0.468	25.0	1.9

than the experimental values and thus considerably lower than our own. The freezing density is 20% lower, and the melting density is 10% lower than our values. On the basis of variational calculations, the volume difference between the two phases has always turned out to be much too large. Hansen and Pollock quote a value of 4.5 cm^3/mole, this is to be compared with 1.9 cm^3/mole found experimentally and our own result of 1.6 cm^3/mole.

It is quite striking that all variational estimates have yielded transition densities below the experimental values. There may be a simple explanation of this, i.e., that the variational calculations always produce better, that is lower, bounds for the energy of the crystal phase as compared with the fluid phase. The configuration space of the crystal is simpler than of the fluid and one can therefore more readily construct a good trial function for the crystal. In other words there is a basic asymmetry in the variational results for the two phases; energetically they always tend to favor the crystal phase. It follows that the variational results will tend to produce transition densities below the experimental values. We have stressed this point in previous papers.[26] On the other hand there is no reason to suppose that the GFMC method does not do equally well for both phases and produces essentially exact results for both.

We close this section with a brief discussion of Lindeman's ratio for this quantum system. This ratio is defined as $\langle r^2\rangle^{1/2}/d$, where d is the nearest-neighbor distance. For other quantum systems[6,20] it has been established that the Lindeman ratio lies between 0.27 and 0.30 at the melting density. Our own exact GFMC work on the Yukawa system also produced a value in this range. The data we have for $\langle r^2\rangle$, see Table XII, can be used to compute this ratio at our melting density ($\rho\sigma^3=0.512$). We find a value of 0.267 ± 0.0026, lying within the established range. We tentatively conclude that there is a quantum version of Lindeman's classical "melting rule": the ratio $\langle r^2\rangle^{1/2}/d$ always lies in the range 0.27–0.30 for all potentials for which freezing take place.

C. Single-particle density

In a crystal the single-particle density $\rho(r)$ is of considerable interest. The variational studies of quantum crystals have nearly always computed this quantity and insights have been gained from such results.

Since our computations reveal that there is a well defined lattice structure we expect the $\rho(\vec{r})$ will have the periodicity of the crystal. We see no exchange of particles in our GFMC runs; each particle appears to be confined to a region around a lattice site. In these circumstances we can confine our attention to $\rho(\vec{r})$ in the neighborhood of a single lattice site.

Figure 25 shows $\rho(|\vec{r}|)$ at three different densities. Here $\rho(|\vec{r}|)$ is the spherical average of $\rho(\vec{r})$. Table XII lists the second moment of $\rho(\vec{r})$ and a linear combination $\bar{\beta}$ of the fourth moment and the square of the second. The second moment decreases as the density increases; the particles become more localized. If the distribution $\rho(\vec{r})$ were strictly Gaussian then the quantity $\bar{\beta}$ in column six should be zero. We computed $\bar{\beta}$ to obtain a measure of how much the single-particle distribution deviates from Gaussian. Unfortunately the variational and mixed values of $\bar{\beta}$ (see Sec. II D) are rather far apart at all densities. Thus the extrapolated values are not reliable estimates of the exact values of $\bar{\beta}$. From our present computations we conclude that in the density range $\rho\sigma^3=0.468-0.589$, $\bar{\beta}$ lies in the range from $0-1.8\times10^{-3}$. An examination of the variational and mixed values of $\bar{\beta}$ suggests that at low densities there are small positive deviations from Gaussian behavior. Figure 26 shows $\rho(r)$ on a semilog plot. The small deviations from Gaussian behavior are just discernable at the tail of the distribution.

We have not in this work attempted to enlarge our computations to study whether particles are interchanging positions or other more complex motions are taking place. There are two difficulties in such a study. First, for stiff core potentials these motions are likely to be very infrequent so that very long runs may be necessary to observe them. For a soft-core potential, such as the Yukawa, interchanges take place more frequently and can be observed in a GFMC run.[26] Second,we need to modify the importance function to make it completely symmetric,[26] which requires still more computations. We have computed $\rho(\vec{r})$ in nine different directions. These distributions are identical within our errors. Detailed contour plots around a lattice site were also made and these revealed no significant asymmetry. We conclude that over the range of densities we have studied that $\rho(\vec{r})$ is spherically symmetric. Table XIII shows various averages computed with $\rho(\vec{r})$ and leads again to the conclusion that the distribution is extremely symmetric. Whether $\rho(\vec{r})$ will remain spherical at higher densities is an open question.

Unfortunately, KLV did not compute the single-particle distribution in the crystal phase, so no comparison with the hard-sphere system is possible. Turning now to the variational work on the Lennard-Jones system, the papers by Hansen and Levesque[49] and by Hansen[44] both contain information on $\rho(\vec{r})$. Hansen and Levesque present data on the second moment of $\rho(\vec{r})$. When a numerical error is corrected in their data,[50] their values for the second moment agrees with Hansen's. Unfortunately neither paper contains any estimates of the errors in the second moment. A comparison of our results

TABLE XII. Moments of the single-particle distribution function. The first column gives the density in reduced units. The next three columns give the second, fourth, and sixth moments of the single-particle distribution. $\bar{\beta} = \langle r^4 \rangle - \frac{5}{3}\langle r^2 \rangle^2$. All lengths are in units of σ. A measure of the departure of the single-particle distribution from Gaussian form is $\bar{\beta}/\langle r^2 \rangle^2$.

$\rho\sigma^3$	$\langle r^2 \rangle$	$\langle r^4 \rangle$	$10\langle r^6 \rangle$	$\bar{\beta}/25$
0.468	0.157 ± 0.002	0.042 ± 0.002	0.153 ± 0.014	$(0.169 \pm 0.154) \times 10^{-4}$
0.526	0.127 ± 0.002	0.029 ± 0.001	0.096 ± 0.006	$(0.684 \pm 0.179) \times 10^{-4}$
0.589	0.099 ± 0.003	0.016 ± 0.001	0.037 ± 0.003	$\sim 10^{-6}$

with these variational data reveals that at the two lowest densities, $\rho\sigma^3 = 0.468$ and 0.526, our values are about 10% larger. At the highest density $\rho\sigma^3 = 0.589$ the values are, within our errors, the same.

We next turn to a comparison of our results for $\rho(\vec{r})$ with those found in a detailed study of the classical hard-sphere crystal.[51] We have little doubt that a classical Lennard-Jones crystal would behave in a very similar way to the hard-sphere crystal. Hence we feel confident in making this comparison which reveals interesting differences between the classical and quantum systems.

It is of course well known that the particles in a classical system tend to be much more localized than those in a quantum system. This is confirmed by the direct simulation of Young and Alder.[51] Near the melting density the ratio of root-mean-square displacement to the nearest-neighbor distance of the classical system is close to one half that of the quantum Lennard-Jones system near melting. Two other qualitative points are interesting. The classical system shows distinct non-Gaussian behavior for $\rho(\vec{r})$. At low densities $\rho(\vec{r})$ drops off more slowly than a Gaussian, while at high densities it falls off somewhat faster. As we have just pointed out, the moments of our distribution cannot be reliably extrapolated to give an estimate $(\bar{\beta})$ of non-Gaussian behavior. The values of $\bar{\beta}$ from both variational and mixed computations suggest small positive deviations of about 5% from Gaussian behavior. This is comparable with those found by Alder and Young in the classical

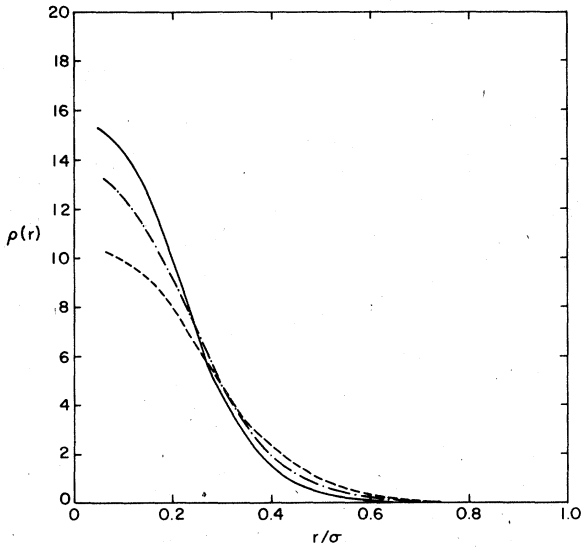

FIG. 25. Single-particle density at three densities in the crystal phase. The solid curve is for the density $\rho = 0.589\sigma^{-3}$, the dashed and dotted curve for $\rho = 0.526\sigma^{-3}$, and the dashed curve for $\rho = 0.468\sigma^{-3}$.

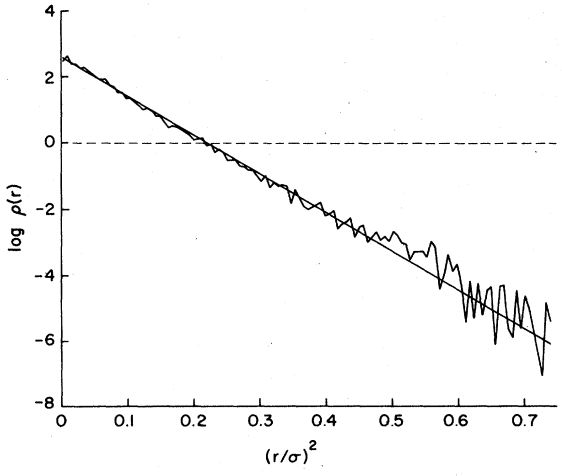

FIG. 26. Semilog plot of the single-particle density $\rho(r)$ in the crystal phase at a density $\rho = 0.526\sigma^{-3}$. The straight line represents a perfect Gaussian distribution with the same second moment as $\rho(r)$.

TABLE XIII. Moments of the single-particle distribution function in the crystal phase. The first column gives the density in reduced units. The quantities in pointed brackets have been averaged over the single-particle distribution function $\rho(\vec{r})$. A completely isotropic distribution would lead to identical values for all entries at a given density. The small differences between the entries at a given density are within our computational errors.

$\rho\sigma^3$	$\langle\|x\|\rangle$	$\langle\|y\|\rangle$	$\langle\|z\|\rangle$	$\langle\|x+y\|\rangle$	$\langle\|x-y\|\rangle$	$\langle\|x+z\|\rangle$	$\langle\|x-z\|\rangle$	$\langle\|y+z\|\rangle$	$\langle\|y-z\|\rangle$
0.468	0.537	0.536	0.531	0.534	0.538	0.540	0.528	0.536	0.530
0.526	0.436	0.426	0.419	0.452	0.411	0.411	0.444	0.417	0.428
0.589	0.352	0.323	0.332	0.342	0.333	0.351	0.333	0.322	0.333

hard-sphere system near melting. Our data at the highest density suggest a much smaller value than 5%. Our results only cover the density range from melting up to 25% above melting, whereas the hard-sphere results go up to 40% above melting. Clearly a comparison over a wider density range would be desirable. Second, the classical hard-sphere results show considerable anisotropy for $\rho(\vec{r})$. This anisotropy is present, but weak, at low densities and becomes very pronounced at higher densities. This is markedly different behavior from our results which, as we have noted, show highly spherical distributions. Again a comparison over a wider density range would be interesting. It is likely that the comparatively large amplitude oscillations in the quantum system effectively average out any tendency to an anisotropic distribution.

We close this section with a discussion of the type of localization that appears in our GFMC simulations. It has already been pointed out that the particles remain localized in the neighborhood of the lattice sites. A detailed examination of the probability distribution around individual sites reveals two novel features. First, there is a definite tendency for the *average position* of the particle to move away from the original lattice site. These deviations from the original sites are nearly always small and random in direction. Second, in a few instances the deviation is large and quite striking. Figure 27 shows the distribution of the centers of mass of all the particles of the crystal accumulated over five of our usual GFMC runs. Clearly there is a significant spread representing particles whose centers of mass have deviated sharply from the original sites. On the same graph we have

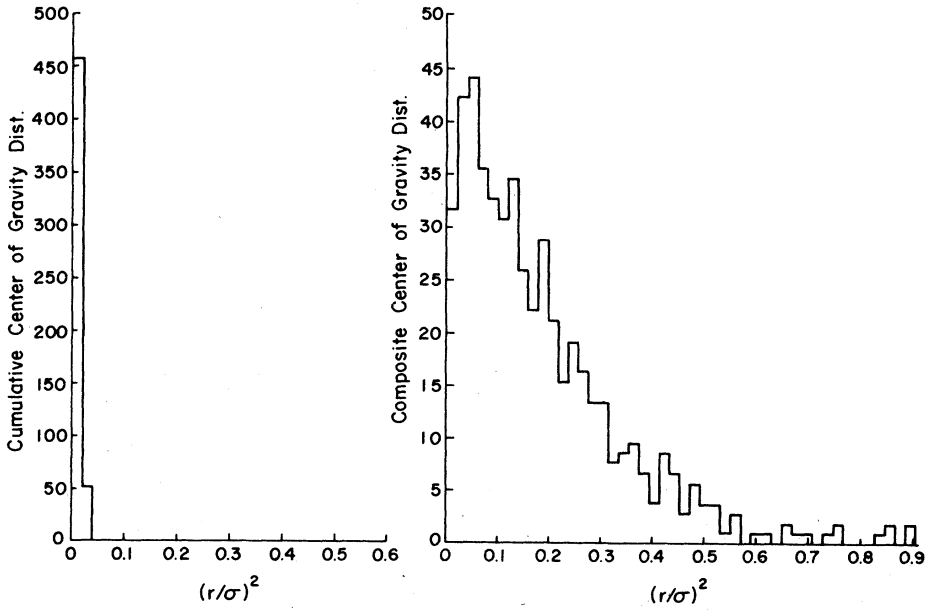

FIG. 27. Distribution of the center of gravities of the particles in the crystal phase. The left curve is the distribution from a variational calculation. The right curve is the distribution from our GFMC calculation. Both are for a density $\rho=0.526\sigma^{-3}$.

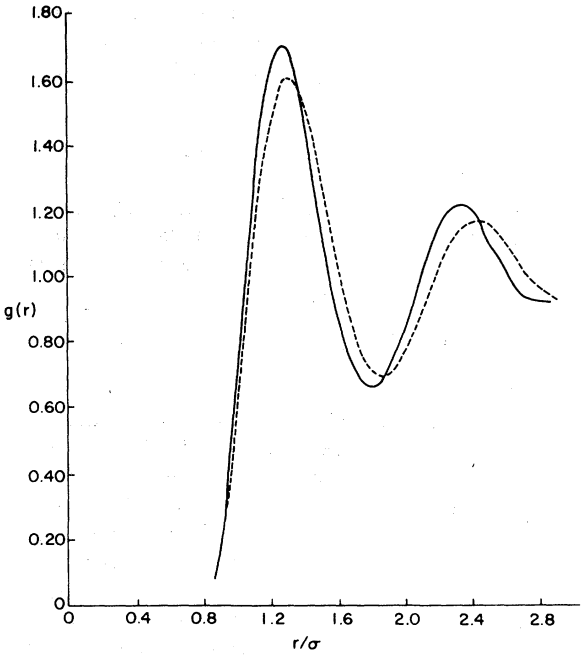

FIG. 28. Radial distribution function $g(r)$ in the crystal phase. The dashed curve is for a density $\rho=0.526\sigma^{-3}$, the solid curve for a density $\rho=0.589\sigma^{-3}$.

plotted the distribution obtained by a variational calculation of the usual kind. The difference is striking; the variational wave function allows very little motion of the center of masses from the lattice sites. On the other hand the GFMC method allows much more freedom for the particles and this gives rise to the long tail we observe. We are not aware of any other studies of these phenomena in other classical or quantum systems. The results we presented earlier on the single-particle distribution functions were obtained by averaging over all the particles in the system. Since the deviations from the lattice sites are random in direction they average out in the final distribution.

D. Pair correlation and structure function

As far as we are aware there are no published data on $S(k)$ or $g(r)$ for the crystal phase. Both of these correlation functions will of course show directional dependence. We thought it worthwhile to present data for the spherical average of both these functions at our two highest densities $\rho\sigma^3=0.526$ and 0.589.

Figure 28 shows $g(r)$ at two densities. As the density increases there is a rapid rise in the height of the first peak of this function. This is due to the sharper localization of the particles which we noted in Sec. IV C. However the degree of correlation revealed by these curves is still relatively weak. For example, in the *fluid* phase the classical Lennard-Jones system has a pair correlation function with a first peak height which is often greater than 3.0, as compared with our value of 1.7. As far as we are aware there have been no published variational results giving $g(r)$ for quantum crystals.

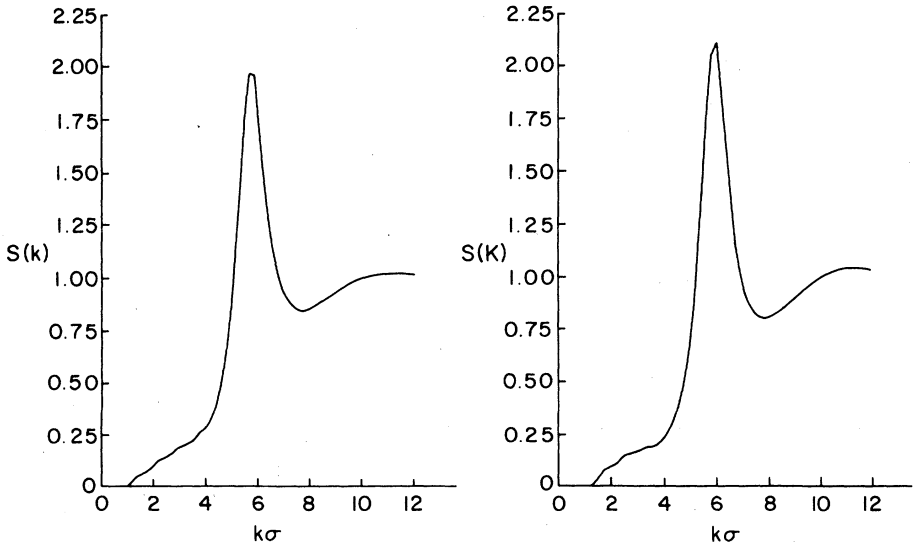

FIG. 29. Structure factor $S(k)$ in the crystal phase. The left curve is for a density $\rho=0.526\sigma^{-3}$, the right curve is for a density $\rho=0.589\sigma^{-3}$.

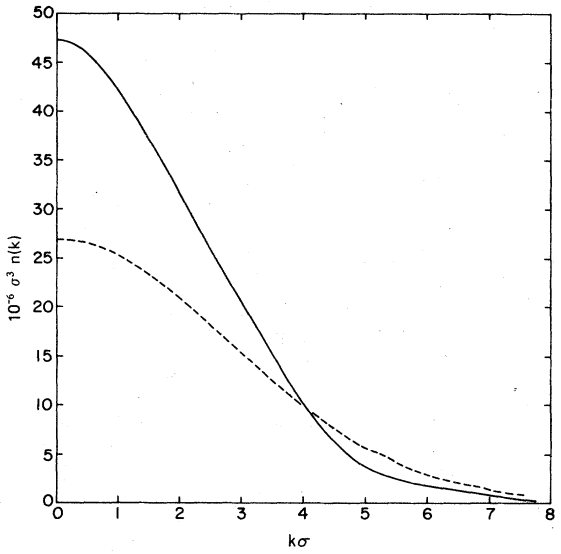

FIG. 30. Momentum distribution in the crystal phase compared with that in the fluid phase. The solid curve is for the fluid phase at $1.2\rho_0(\rho=0.438\sigma^{-3})$ the dashed curve for the crystal phase at $\rho=0.526\sigma^{-3}$.

Figure 29 shows our sphericalized structure functions at the same densities. The rising of the first peak with increasing density again reflects, although more indirectly, the increasing order in the system. However, as with $g(r)$, $S(k)$ reveals comparatively weak order. It is well known that $S(k)$ has a first peak height of 2.85 near freezing for many classical systems. The highest value, at a density 25% above freezing, of the first peak is 1.97. We would welcome experimental data on $S(k)$ in the crystal phase. It is likely that it will provide a sensitive test of the two-body potential used in our GFMC calculations.

E. Momentum distribution

We have computed both the single-particle density matrix and its Fourier transform $n(k)$ in the crystal phase. No data, corresponding to those available in the fluid phase, have been published for the crystal. Nevertheless, we present data at one typical density.

When we extrapolate $\rho_1(r)$ to large r we find, for all densities in the crystal phase, that it extrapolates accurately to zero. We thus conclude that within our errors there is no condensate fraction in the crystal. Of course we cannot rule out the presence of a small condensate less than our error estimate which is about 1%. We can, however, say that there is a rapid drop in the condensate fraction as we move from the high-density fluid phase to the low-density crystal phase. We remark that for the soft Yukawa potential our GFMC studies[20] have shown condensate fractions of the order of a few percent in the crystal phase. Whether the absence of a condensate in the helium crystal is a consequence of the type of importance function we have used in our GFMC calculations is a matter which must await more extensive calculations.

Figure 30 shows the sphericalized momentum distribution for $\rho\sigma^3=0.526$. On the same graph we show the momentum distribution for the highest fluid density. In the denser crystal phase the distribution is much wider. This is to be expected as the kinetic energy of the system has risen from 19 to 27 °K per particle, a consequence of the increased localization of the particles. We would welcome measurements of $n(k)$, as a function of density, in the solid phase.

V. SUMMARY AND CONCLUSIONS

We have given a survey of the properties of liquid and crystal phases of ^{4}He modeled as a boson system with a Lennard-Jones potential. Although we have repeated certain variational calculations with product ("Jastrow") wave functions, the principal tool was the Green's-function Monte Carlo method. It has been shown that this method is reliable, giving results which are independent of importance functions that differ significantly. The errors, statistical and other, of our numerical results were carefully assessed. Energy values can be obtained with errors less than 1%; these are exact except for statistical errors, minor numerical errors, and a somewhat uncertain but small size dependence. Properties derived from the energy such as pressure, velocity of sound, and compressibility of the solid have larger errors but are good enough for quantitative comparison with experiment. Quantum-mechanical expectations have generally been computed using the "extrapolation" method. The latter is not exact—it gives in fact stationary estimates, but the results for structure function, $g(r)$, momentum density, and crystal one-body distribution have been demonstrated to be independent of trial functions from which the expectations are made.

The new calculations confirm definitively that the equation of state of liquid and fcc crystal phases are substantially lower in energy than given by product trial functions. The agreement with experiment is considerably improved but we conclude that the Lennard-Jones potential with de Boer–Michels parameters does not give a quantitative description of condensed helium. The structure function for the fluid, on the other hand, is in good agreement with experiment when evaluated at the calculated equilibrium density which coincides with the experimental value. The calculated momentum distribution agrees reasonably well with recent analyses of neutron

scattering data although neither set of data is extremely precise. Our estimate of the average kinetic energy conforms closely to a recent experimental estimate. Finally we estimate a condensate fraction of 0.11 at equilibrium. Woods and Sears[43] derived a value of 0.069 ± 0.008 from neutron scattering experiments at 1.1 °K. We suggest that additional experimental information on this and on the momentum distribution at other fluid densities would be well worthwhile.

One can draw useful theoretical conclusions as well. The first is that within their errors, we confirm the predictions of Kalos, Levesque, and Verlet[6] for the energy of the LJ fluid based upon their perturbation theory connecting hard-sphere and hard-core systems. This, in turn, permits us to make preliminary predictions of the fluid equation of state which would be given by alternative two-body potentials[9] that have been proposed in the literature. Specifically, using the KLV perturbation theory we find the LJ II[45] potential has the wrong shape for the equation of state. The Beck and the Bruch-McGee I potential[9] gives energy values which seem too shallow. The exponential-Spline-Morse-Morse-Spline-Van der Waals (ESMMSV) potential[52] may also give shallower energies than LJ potential. The Bruch-McGee II potential may be excluded on the basis of simple perturbation theory which gives an upper bound of −8.4 °K per particle at $\rho = \rho_0$.

It seems likely that the deficiency of the Jastrow trial function in predicting accurately ground-state properties of condensed helium is its omission of certain significant three-body correlations. Their inclusion in approximate treatments of the variational calculation[5,7] has lowered the predicted energy nearly to the value predicted by the GFMC method.

Our conclusions about solid ^{4}He are generally similar to those for the fluid except that fewer experimental data exist. Again the equation of state calculated by GFMC is in better agreement with experiment than is that calculated variationally with trial functions consisting of a Jastrow product times localization factors at each lattice site. Nevertheless, the Lennard-Jones potential is clearly in error. The disagreement cannot be explained by the differences between fcc and hcp phases. In repeating variational calculations for the fcc lattice, we have improved the statistics to the point where, in the density range considered the differences between the energies of the two types of crystal orders are less than 0.1 °K, the Monte Carlo error. We plan GFMC calculations for the hcp phase and for whatever force law appears best as calculated by hard-sphere perturbation theory.

To confirm these accurate calculations of properties of solid ^{4}He it would be very useful if experimental measurements of structure functions, momentum distributions and average kinetic energy could be carried out.

ACKNOWLEDGMENTS

The authors would like to thank the Aspen Center for Physics for their hospitality during the writing of this paper. We are also grateful to M. Rao for valuable contributions to this work. This paper was supported by the U. S. DOE under Contract No. EY-76-C-02-3077*000 and by the NSF under Grant No. DMR-77-18329.

APPENDIX A: ESTIMATION OF THREE-BODY POTENTIAL

We have estimated the perturbation of the energy arising from the Axilrod-Teller[11] triple-dipole potential

$$V_3(r_{12},r_{13},r_{23}) = \frac{0.324\left(1+3\prod_{i=1}^{3}\cos\theta_i\right)}{r_{12}^3 r_{13}^3 r_{23}^3} . \quad \text{(A1)}$$

The coefficient is such that V_3 gives an energy in °K when r is expressed in units of σ. Our estimates were obtained as follows. The most important contribution, in which all r_{ij} are less than half the side of the periodic box L may be computed directly from configurations (i.e., sets of numerical values of coordinates of all particles) recorded on magnetic tape for both variational and GFMC runs. Since this requires three-body sums it is moderately time consuming. After a little experimentation it was found that accuracy of the order of 0.002 °K or better, could be obtained from 100 sparsely chosen configurations for each case. To compute the errors in $\langle V_3\rangle$ GFMC averages were obtained from configurations recorded from two nonconsecutive runs. Extrapolated values of $\langle V_3\rangle$ were obtained from the GFMC (i.e., "mixed") estimates and from the variational estimates by means of the usual extrapolation

$$\langle V_3\rangle_{\text{ex}} = 2\langle V_3\rangle_M - \langle V_3\rangle_T . \quad \text{(A2)}$$

A significant tail correction, where some $r_{ij} > \frac{1}{2}L$, remained to be estimated. This was done by a Monte Carlo quadrature in which the superposition approximation was made

$$\rho_3(\vec{r}_1,\vec{r}_2,\vec{r}_3,) = \rho^3 g(\vec{r}_{12})g(\vec{r}_{13})g(\vec{r}_{23}) \quad \text{(A3)}$$

and in which g was taken to be the extrapolated function for $r < \frac{1}{2}L$ and unity for $r \geq \frac{1}{2}L$. It proved convenient to split the tail correction into that part in which $r_{12} < \frac{1}{2}L$ and $r_{13} > \frac{1}{2}L$, and that part in which both r_{12} and r_{13} exceed the cutoff. For the first integral, a trapezoidal integration over r_{12} was combined with Monte Carlo integration on r_{13} and on the cosine of the angle θ_1, between r_{12} and r_{13}.

The variable r_{13} was sampled from a probability

distribution function[53] $q_4(r_{13})$ proportional to r_{13}^{-4}, with $r_{13} > \frac{1}{2}L$. The variable $\cos\theta$ was sampled uniformly. Both r_{13} and $\cos\theta_1$ were stratified[54] as well, using of the order of ten intervals.

For the integral in which r_{12} was also larger than $\frac{1}{2}L$ the procedure was the same except that r_{12} was also sampled in a stratified way from $q_4(r_{12})$. A few seconds of computing gave statistical errors for the combined tail correction of less than 0.001 °K.

A useful check on the tail correction was provided by carrying out the procedure for the 64 and 128 body results at $\rho = 0.9\rho_0$. For 64 particles the extrapolated $\langle V_3\rangle$ is 0.1128 °K with an estimated tail correction of 0.0077 for a total $\langle V_3\rangle$ of 0.1205 ± 0.0016. The corresponding results obtained with 128 particles were 0.1161, 0.0034, and 0.1195 ± 0.0017. The two results agree satisfactorily within statistical errors. The discrepancy of 0.001 °K is about 13% of the 64 body tail correction but is completely negligible as far as total energy is concerned. For 64 particles the tail correction is about 8% of the total $\langle V_3\rangle$ for every fluid density and 4–5% of $\langle V_3\rangle$ for crystal states.

APPENDIX B: PHONON CORRECTION

The Green's-function Monte Carlo method is exact for a finite system. In this section we attempt to correct for the finite size of our simulation cell by including the correlations introduced by the zero-point motion of the long-wavelength phonons which would be present in an infinite system. One knows for example that the structure function for small k will behave like

$$\lim_{k\to 0} S(k) = \frac{\hbar k}{2mc} , \tag{B1}$$

where c is the speed of sound and m is the mass of a helium atom. The Monte Carlo results will not satisfy this condition since the k's are limited by the periodic boundary conditions to be in the reciprocal lattice of the simulation cell.

It has been proposed by Reatto and Chester[55] that one can correct for the finite system size by assuming that the infinite-system wave function ψ_∞ is related to the finite-system wave function ψ_N by

$$\psi_\infty = \psi_{\text{phonon}}\psi_N , \tag{B2}$$

where,

$$\psi_{\text{phonon}} = \exp\left[-\tfrac{1}{2}\sum_{i<j}\frac{mc}{\pi^2\rho\hbar}(r_{ij}^2 + k_c^{-2})^{-1}\right] = \exp\left[-\tfrac{1}{2}\sum_{i<j} u_{LR}(r_{ij})\right] . \tag{B3}$$

This phonon wave function gives the correct behavior of $S(k)$ at small k [Eq. (B1)]. The parameter k_c can be varied to minimize the energy but it should correspond only to long-wavelength phonons, i.e.,

$$k_c L \lesssim 1 \quad \text{and} \quad k_c\sigma \ll 1 . \tag{B4}$$

To calculate the change in $g(r)$, and hence in $S(k)$ and the energy, the reference-hypernetted-chain equation (RHNC) is used. Let $\Delta S(k) = S_\infty(k) - S_N(k)$ where S_N is calculated using an N-body system. Then the change in the direct correlation function is

$$\Delta C(k) = \frac{\Delta S}{S_N^2(k) + \Delta S(k) S_N(k)} \tag{B5}$$

and the RHNC equation is

$$\Delta C(r) = \Delta g(r) - u(r) - \ln\left[1 + \frac{\Delta g(r)}{g_N(r)}\right] . \tag{B6}$$

For a given $u(r)$ and $g_N(r)$ these equations can be iterated to yield $\Delta S(k)$ and $\Delta g(r)$. It should be noted that both $g_\infty(r)$ and $S_\infty(k)$ will be positive and the small k condition in Eq. (B1) will be exactly satisfied.

Now the ground-state energy is approximately given by its variational estimate

$$E = \frac{\rho}{2}\int d^3r\, g(r)\left[V(r) + \frac{\hbar^2}{2m}\nabla^2 u_{SR}(r)\right] , \tag{B7}$$

where

$$u_{SR} = \tfrac{1}{2}(b/r)^5 . \tag{B8}$$

Then the change in energy will be

$$\Delta E = E_\infty - E_N = \frac{\rho}{2}\int d^3r\, \Delta g(r)\left[V(r) + \frac{\hbar^2}{2m}\nabla^2 u_{SR}\right] + \frac{\rho}{2}\int d^3r\, g_N(r)\frac{\hbar^2}{2m}\nabla^2 u_{LR}(r) . \tag{B9}$$

The change in energy resulting from this procedure is very small. For example at the density of

$$\rho = 0.3648/\sigma^3 , \quad \Delta E = -2.7\times 10^{-4}\ ^\circ\text{K}$$

(with $C = 237$ m/sec and $k_c = 0.144/\sigma$). The energy shift can be lowered somewhat more by varying the speed of sound as well; the minimum occurs when $c = 950$ m/sec, $k_c = 0.105/\sigma$, and $\Delta E = -3.5\times 10^{-4}$ °K. At higher densities the shift is larger; for example at

$$\rho = 0.49/\sigma^3 , \quad \Delta E = -2.3\times 20^{-3}\ ^\circ\text{K}$$

(with $c = 475$ m/sec and $k_c = 0.25/\sigma$). These ener-

gies are much smaller than the errors in the calculation and can be completely ignored. Similarly the change in $S(k)$ is significant only at very small k. Thus far we have merely estimated the change in the variational energy due to ψ_{phonon}. In essence what we have done is to estimate the magnitude of a very small size-dependent term in the variational energy. The size dependence comes about because as we increase the size of the system more and more long-wavelength phonon modes are included in the variational calculation. By resorting to an approximate integral equation (RHNC) we have been able to estimate the size of the correction for an arbitrary large system.

Unfortunately this procedure cannot be carried out within the framework of the GFMC method. The procedure depends on an explicit knowledge of the wave function, which we do not have. However we see no reason to believe that the magnitude of the effect would be significantly different for a variational calculation as compared with a GFMC calculation. This statement is confirmed by the tests for size dependence in our GFMC studies. It will be recalled from our discussion in Sec. II C that there was no appreciable size dependence in the energy of the system. We thus conclude that as we include more phonon modes into the GFMC calculation the energy is not appreciably changed.

It should be mentioned that in an earlier calculation[6] with the GFMC method on hard spheres, the "phonon correction" is in error (the tail correction to $\nabla^2 u_{LR}$ was neglected). When the error is rectified[56] the energy shift is roughly $10^{-3}(\hbar^2/ma^2)$; compare Table I and Fig. 1 of Ref. 6.

APPENDIX C: EXTENSION OF THE RADIAL DISTRIBUTION FUNCTION

The radial distribution function $g(r)$ obtained in a simulation is naturally limited to values of r less than half of the simulation box size, i.e., $r \leq \frac{1}{2}L$. To compute the structure function $S(k)$ one needs to make an extension to larger values. The simplest assumption, namely, $g(r)=1$ for $r > \frac{1}{2}L$, often leads to a physically unacceptable $S(k)$ for small k, for example, an $S(k)$ which is negative.

To extend the $g(r)$ to large r we have assumed that for $r > \frac{1}{2}L$, g is well approximated by $\tilde{g}$ which describes damped oscillations,

$$\tilde{g}(r) = 1 + (1/r)\,\mathrm{Re}(Ae^{z/r}) \quad . \tag{C1}$$

Here A and z are complex parameters determined by a nonlinear fit which minimizes χ^2 where,

$$\chi^2 = \int_{r_0}^{L/2} d^3r\,[g_{\text{MC}}(r) - \tilde{g}(r)]^2 \tag{C2}$$

$g_{\text{MC}}(r)$ is the radial distribution function generated by our Monte Carlo runs. The lower limit to the fit r_0 was located near the first minimum of $g_{\text{MC}}(r)$.

This method of extending $g(r)$ was previously used and tested on the classical one component plasma[57] at very high density where $g(r)$ displays much more correlation than for ^{4}He, and was found to give very reliable results. We believe the assumed form of $g(r)$ is reasonable for ^{4}He since the values for χ^2 compared well with the small statistical errors in $g_{\text{MC}}(r)$. In addition $S(k)$, obtained from Fourier transforming the extended g, is well behaved for small k.

APPENDIX D: TABULATED RADIAL DISTRIBUTION AND STRUCTURE FUNCTIONS

In this Appendix we present Tables XIV–XVII for $g(r)$ and $S(k)$ at several densities.

TABLE XIV. Radial distribution function $g(r)$ for three densities [r is in units of σ and denotes the upper end of the interval for which $g(r)$ is given].

r	ρ_0	$1.1\rho_0$	$1.2\rho_0$	r	ρ_0	$1.1\rho_0$	$1.2\rho_0$
0.6800	0.0000	0.0000	0.0000	1.1200	0.8542	0.9539	0.9971
0.7200	0.0001	0.0002	0.0002	1.1600	1.0158	1.1013	1.1541
0.7600	0.0007	0.0002	0.0016	1.2000	1.1229	1.2322	1.2676
0.8000	0.0038	0.0059	0.0056	1.2400	1.2353	1.2830	1.3652
0.8400	0.0171	0.0211	0.0262	1.2800	1.2976	1.3555	1.3920
0.8800	0.0562	0.0559	0.0637	1.3200	1.3082	1.3682	1.4139
0.9200	0.1250	0.1431	0.1487	1.3600	1.3488	1.3857	1.4193
0.9600	0.2253	0.2586	0.2793	1.4000	1.3226	1.3482	1.4140
1.0000	0.3550	0.4131	0.4366	1.4400	1.3103	1.3234	1.3444
1.0400	0.5078	0.6010	0.6463	1.4800	1.2837	1.2694	1.3007
1.0800	0.6854	0.7915	0.8818	1.5200	1.2331	1.2132	1.2413

TABLE XIV. *(Continued)*

r	ρ_0	$1.1\rho_0$	$1.2\rho_0$	r	ρ_0	$1.1\rho_0$	$1.2\rho_0$
1.5600	1.2287	1.1609	1.1696	2.1600	0.9096	0.9306	0.9216
1.6000	1.1678	1.1243	1.1362	2.2000	0.9195	0.9464	0.9240
1.6400	1.1256	1.0835	1.0654	2.2400	0.9287	0.9581	0.9495
1.6800	1.1009	1.0539	1.0302	2.2800	0.9529	0.9742	0.9744
1.7200	1.0393	1.0060	0.9771	2.3200	0.9682	0.9998	1.0053
1.7600	1.0065	0.9548	0.9445	2.3600	0.9757	1.0047	1.0182
1.8000	0.9854	0.9414	0.9082	2.4000	1.0020	1.0206	1.0401
1.8400	0.9513	0.9187	0.8853	2.4400	1.0074	1.0280	1.0516
1.8800	0.9520	0.9036	0.8788	2.4800	1.0105	1.0407	1.0589
1.9200	0.9231	0.8983	0.8550	2.5200	1.0281	1.0418	1.0531
1.9600	0.9036	0.8888	0.8517	2.5600	1.0317	1.0323	1.0690
2.0000	0.8955	0.8754	0.8676	2.6000	1.0364	1.0330	1.0560
2.0400	0.9118	0.8970	0.8546	2.6400	1.0298	1.0398	1.0522
2.0800	0.8987	0.9023	0.8791	2.6800	1.0393	1.0386	1.0597
2.1200	0.9105	0.9096	0.9064				

TABLE XV. Structure function $S(k)$ at three densities (k is in units of σ^{-1}).

k	ρ_0	$1.1\rho_0$	$1.2\rho_0$	k	ρ_0	$1.1\rho_0$	$1.2\rho_0$
0.2	0.089	0.045	0.037	6.2	1.129	1.185	1.211
0.4	0.091	0.048	0.036	6.4	1.084	1.128	1.142
0.6	0.096	0.054	0.041	6.6	1.046	1.079	1.084
0.8	0.103	0.063	0.050	6.8	1.016	1.037	1.038
1.0	0.113	0.075	0.061	7.0	0.991	1.004	1.002
1.2	0.124	0.088	0.072	7.2	0.972	0.978	0.973
1.4	0.137	0.104	0.086	7.4	0.959	0.959	0.952
1.6	0.152	0.122	0.102	7.6	0.950	0.946	0.937
1.8	0.170	0.141	0.120	7.8	0.944	0.937	0.928
2.0	0.190	0.163	0.138	8.0	0.942	0.933	0.923
2.2	0.212	0.186	0.158	8.2	0.942	0.932	0.922
2.4	0.237	0.211	0.181	8.4	0.945	0.934	0.925
2.6	0.264	0.238	0.205	8.6	0.950	0.938	0.930
2.8	0.296	0.269	0.230	8.8	0.955	0.944	0.936
3.0	0.332	0.302	0.257	9.0	0.962	0.952	0.945
3.2	0.375	0.341	0.289	9.2	0.970	0.960	0.954
3.4	0.426	0.386	0.325	9.4	0.977	0.968	0.964
3.6	0.487	0.441	0.367	9.6	0.985	0.977	0.974
3.8	0.564	0.508	0.420	9.8	0.992	0.985	0.984
4.0	0.659	0.591	0.491	10.0	0.998	0.993	0.993
4.2	0.774	0.693	0.584	10.2	1.004	1.000	1.001
4.4	0.908	0.817	0.707	10.4	1.008	1.006	1.008
4.6	1.051	0.958	0.869	10.6	1.012	1.011	1.013
4.8	1.181	1.102	1.063	10.8	1.015	1.015	1.017
5.0	1.274	1.229	1.255	11.0	1.016	1.018	1.020
5.2	1.318	1.317	1.397	11.2	1.017	1.019	1.022
5.4	1.316	1.354	1.456	11.4	1.017	1.020	1.022
5.6	1.282	1.344	1.436	11.6	1.016	1.019	1.021
5.8	1.232	1.302	1.370	11.8	1.015	1.018	1.020
6.0	1.179	1.245	1.289	12.0	1.013	1.016	1.017

TABLE XVI. Single-particle density in the crystal phase.

$\rho = 0.526\sigma^{-3}$

r	$\rho(r)$	r	$\rho(r)$	r	$\rho(r)$	r	$\rho(r)$
0.05640	13.24400	0.40277	1.83520	0.56681	0.30074	0.69305	0.05767
0.09769	12.43200	0.41059	1.68100	0.57239	0.28050	0.69762	0.05939
0.12611	11.62000	0.41827	1.57560	0.57792	0.25956	0.70216	0.05804
0.14922	11.01073	0.42580	1.51540	0.58340	0.24706	0.70668	0.05733
0.16920	10.20620	0.43321	1.39780	0.58883	0.23138	0.71117	0.05504
0.18706	9.66560	0.44049	1.29300	0.59420	0.20388	0.71563	0.05078
0.20335	8.95100	0.44766	1.22460	0.59953	0.17590	0.72006	0.04439
0.21843	8.39620	0.45471	1.13644	0.60481	0.17294	0.72446	0.03959
0.23254	7.78340	0.46165	1.06726	0.61005	0.15418	0.72884	0.03743
0.24584	7.13200	0.46849	0.99440	0.61524	0.14826	0.73319	0.03435
0.25845	6.57720	0.47523	0.93572	0.62039	0.14110	0.73752	0.03866
0.27048	6.05700	0.48188	0.85242	0.62550	0.13792	0.74182	0.03954
0.28200	5.61400	0.48843	0.78420	0.63056	0.13488	0.74609	0.03466
0.29306	4.99520	0.49490	0.70966	0.63559	0.11921	0.75034	0.03078
0.30372	4.58460	0.50129	0.67908	0.64057	0.10321	0.75457	0.03122
0.31402	4.18040	0.50759	0.61196	0.64552	0.09940	0.75877	0.02515
0.32399	3.86360	0.51382	0.55526	0.65043	0.09688	0.76295	0.02203
0.33366	3.48120	0.51996	0.52522	0.65530	0.08281	0.76711	0.02247
0.34306	3.28560	0.52606	0.49416	0.66014	0.08352	0.77125	0.01970
0.35221	3.05740	0.53207	0.44948	0.66494	0.08319	0.77536	0.01604
0.36113	2.81420	0.53801	0.41198	0.66970	0.07470	0.77945	0.01298
0.36983	2.63760	0.54389	0.38964	0.67444	0.06601	0.78352	0.01073
0.37834	2.45240	0.54971	0.35338	0.67914	0.06776	0.78757	0.00896
0.38665	2.18620	0.55547	0.32750	0.68380	0.06262	0.79160	0.01042
0.39479	1.97140	0.56117	0.30678	0.68844	0.05749	0.79561	0.00995

TABLE XVII. Single-particle density in the crystal phase.

$\rho = 0.589\sigma^{-3}$

r	$\rho(r)$	r	$\rho(r)$	r	$\rho(r)$	r	$\rho(r)$
0.04974	15.29400	0.35522	2.63320	0.49988	0.37800	0.61122	0.06118
0.08615	14.68900	0.36212	2.40840	0.50481	0.34548	0.61525	0.05678
0.11122	14.08400	0.36888	2.20340	0.50969	0.32992	0.61926	0.04854
0.13160	13.40800	0.37553	2.02260	0.51452	0.30364	0.62324	0.04611
0.14922	12.65800	0.38206	1.85300	0.51930	0.29176	0.62720	0.04321
0.16497	11.59600	0.38848	1.74760	0.52405	0.28220	0.63113	0.04024
0.17934	11.11000	0.39480	1.60320	0.52875	0.26986	0.63504	0.03592
0.19264	10.44400	0.40102	1.48020	0.53341	0.23456	0.63893	0.03001
0.20508	9.80180	0.40714	1.39900	0.53802	0.22100	0.64279	0.02902
0.21681	9.15060	0.41317	1.26094	0.54260	0.20402	0.64662	0.02586
0.22794	8.48660	0.41912	1.16554	0.54714	0.17706	0.65044	0.02278
0.23855	7.65740	0.42498	1.08124	0.55165	0.17862	0.65423	0.01847

TABLE XVII. *(Continued.)*

$\rho=0.589\sigma^{-3}$							
r	$\rho(r)$	r	$\rho(r)$	r	$\rho(r)$	r	$\rho(r)$
0.24870	6.97400	0.43076	1.01968	0.55611	0.16392	0.65800	0.01612
0.25846	6.46340	0.43647	0.93770	0.56055	0.15644	0.66175	0.01645
0.26786	5.82780	0.44210	0.88318	0.56494	0.14298	0.66548	0.01675
0.27694	5.37060	0.44766	0.83444	0.56930	0.13196	0.66919	0.01420
0.28574	5.01300	0.45316	0.76798	0.57363	0.11080	0.67287	0.01540
0.29427	4.72240	0.45858	0.69204	0.57793	0.11124	0.67654	0.01606
0.30256	4.34280	0.46395	0.64356	0.58220	0.10988	0.68019	0.01198
0.31063	4.13240	0.46925	0.64204	0.58643	0.11074	0.68382	0.00854
0.31849	3.77960	0.47449	0.58452	0.59063	0.10400	0.68742	0.00563
0.32617	3.52320	0.47968	0.53776	0.59481	0.09917	0.69101	0.00266
0.33367	3.25220	0.48481	0.51586	0.59895	0.09321	0.69459	0.00000
0.34100	3.05840	0.48989	0.46966	0.60307	0.07791	0.69814	0.00000
0.34818	2.85160	0.49491	0.40998	0.60716	0.06396	0.70167	0.00000

*Present address: NRCC, Lawrence Berkeley Laboratory, Berkeley, CA USA.

[1]Monte Carlo methods for the variational quantum many-body problem where first used by W. L. McMillan, Phys. Rev. A 138, 442 (1965). His results were confirmed by Murphy and Watts, J. Low Temp. Phys. 2, 507 (1970) and by Schiff and Verlet using molecular dynamics, Phys. Rev. 160, 208 (1967). Levesque, TuKiet, Schiff, and Verlet were the first to use the HNC equation in this problem (unpublished). Murphy and Watts (unpublished) also used HNC.

[2]J. G. Zabolitzky, Phys. Rev. A 16, 1258 (1977).

[3]M. H. Kalos, Phys. Rev. A 2, 250 (1970).

[4]C. de Michelis and L. Reatto, Phys. Lett. A 50, 275 (1974).

[5]C. C. Chang and C. E. Campbell, Phys. Rev. B 15, 4238 (1977).

[6]M. H. Kalos, D. Levesque, and L. Verlet, Phys. Rev. A 9, 2178 (1974).

[7]V. J. Pandharipande (private communication).

[8]J. de Boer and A. Michels, Physica (Utrecht) 5, 945 (1938).

[9]J. Barker, *Rare Gas Solids,* edited by M. L. Klein, and J. A. Verables, (Academic, New York, 1976), Chap. IV.

[10]D. M. Ceperley and M. H. Kalos, *Monte Carlo Methods in Statistical Physics,* edited by K. Binder (Springer, Berlin, 1979), Chap. IV.

[11]B. M. Axilrod and E. Teller, J. Chem. Phys. 11, 293 (1943); the coefficient is due to P. J. Leonard (unpublished); quoted by R. D. Murphy and J. A. Barker, Phys. Rev. A 3, 1037 (1971).

[12]Recent simulation studies (see Ref. 20) on crystals of particles interacting via Yukawa potentials have shown that the difference in energy between a symmetric crystal state and an unsymmetric state is of the order of 1%. For a system with a Lennard-Jones potential we expect it to be still smaller.

[13]N. Metropolis, A. W. Rosenbluth, M. N. Rosenbluth, A. M. Teller, and E. Teller, J. Chem. Phys. 21, 1087 (1953).

[14]V_0 is introduced here so that $V(R)+V_0$, which is an effective local absorption rate in the diffusion analog of the Schrödinger equation, is now positive. When importance sampling is introduced [see Eq. (2.10)] V_0 need no longer be a bound on $-V(r)$ but instead, a bound on $-\mathcal{H}\psi_T/\psi_T$, a much smaller number. As we shall see this permits faster convergence; see Ref. 10.

[15]Much of the gross size dependence was eliminated by the method of potential cutoff and by subsequent tail corrections. For a cutoff radius, $r_c \leq \frac{1}{2}L$, we actually used $v'(r)=v(r)-v(r_c)$ for $r \leq r_c$ and $v'(r)=0$ for $r > r_c$. This avoids a discontinuity in v which would perturb the exact solution near r_c. Then a correction was added to make the potential energy equal to $2\pi\rho\int g(r)\,v\,dr$. The assumption that $g=1$ beyond r_c leads to negligible error for fluid states. A correction of about 0.01 °K is needed for the crystal; these are included in Table I and below.

[16]J.-P. Hansen and D. Levesque, Phys. Rev. 165, 293 (1968).

[17]O. Penrose and L. Onsager, Phys. Rev. 104, 576 (1956).

[18]P. R. Roach, J. B. Ketterson, and C. W. Woo, Phys. Rev. A 2, 543 (1970).

[19]S. G. Cochran, Ph.D. thesis (Cornell University, 1976) (unpublished).

[20]A. D. B. Woods and V. F. Sears, J. Phys. C 10, L341(1977).

[21]J. A. Barker and D. Henderson, Rev. Mod. Phys. 48, 587 (1976).

[22]L. J. Lantto, A. D. Jackson, and P. J. Siemans, Phys. Lett. B 68, 311 (1977).

[23]C. E. Campbell and F. Pinski (private communication).

[24]C. de Michelis, G. Massenini, and L. Reatto (unpublished).

[25]C. C. Chang and C. E. Campbell, Phys. Rev. B 13, 3779 (1970).

[26]D. Ceperley, G. V. Chester, and M. H. Kalos, Phys. Rev. B 17, 1070 (1978); D. Ceperley, G. V. Chester, and M. H. Kalos, Phys. Rev. D 13, 3208 (1976).

[27]E. K. Achter and L. Meyer, Phys. Rev. 188, 291 (1969).

[28]W. L. Gordon, C. H. Shaw and J. G. Daunt, Phys. Chem. Solids 5, 117 (1958).

[29]R. A. Cowley and A. D. B. Woods, Can. J. Phys. 49, 177 (1971).

[30]D. G. Hurst and D. G. Henshaw, Phys. Rev. 100, 994 (1955).
[31]D. G. Henshaw, Phys. Rev. 119, 14 (1960).
[32]R. D. Murphy and I. J. McGee, Phys. Lett. A 45, 323 (1973).
[33]R. B. Hallock, Phys. Rev. A 5, 320 (1972).
[34]I. J. McGee and R. D. Murphy, J. Phys. C 5, L311 (1972).
[35]R. A. Cowley and A. D. B. Woods, Phys. Rev. Lett. 21, 787 (1968).
[36]O. K. Harling, Phys. Rev. A 3, 1073 (1971).
[37]H. A. Mook, R. Schern and M. K. Wilkinson, Phys. Rev. A 6, 2268 (1972).
[38]H. A. Mook, Phys. Rev. Lett. 32, 1167 (1974).
[39]H. W. Jackson, Phys. Rev. 185, 186 (1969).
[40]J. F. Fernandez and H. A. Gersch, Phys. Rev. Lett. A 30, 261 (1969).
[41]P. C. Hohenberg and P. M. Platzman, Phys. Rev. 152, 198 (1966).
[42]R. A. Cowley, P. Mantel, E. C. Svensson, A. D. B. Woods, and V. Sears, J. Low Temp. Phys. 23, 285 (1976).
[43]A. D. B. Woods and V. Sears, Phys. Rev. Lett. 39, 415 (1977).
[44]J. P. Hansen, J. Phys. (Paris) 31, C3 67 (1970).
[45]J. P. Hansen and E. L. Pollock, Phys. Rev. A 5, 2651 (1972).
[46]D. O. Edwards and R. C. Pandorff, Phys. Rev. A 140, 816 (1965).
[47]This density dependence was first noted by Hansen and Pollock who also concluded that the Lennard-Jones potential is seriously inadequate in the crystal phase.
[48]The results given in Ref. 44 disagree with the data given in the earlier paper by Hansen and Levesque (Ref. 49). This is because Hansen and Levesque used an inaccurate method to compute the tail connections to the energy. We thank J. P. Hansen for a private communication on this matter.
[49]J. P. Hansen and D. Levesque, Phys. Rev. 165, 293 (1968).
[50]Table III of Ref. 49 has a numerical error in the entries for the root mean square deviation of the particles from the lattice sites. The entries should be multiplied by $3^{1/2}$.
[51]P. A. Young and B. J. Alder, J. Chem. Phys. 60, 1256 (1974).
[52]A. L. J. Burgmans, J. M. Farrar, and Y. T. Lee, J. Chem. Phys. 64, 1345 (1976).
[53]This density function was chosen to match the asymptotic form of the integrand as a function of r_{13}. For $r_{13} >> r_{12}$ and $r_{23} \cong r_{13}$, $v_3 r_{13}^2\, dr_{13} \propto r_{13}^4\, dr_{13}$.
[54]J. M. Hammersley and D. C. Handscomb, *Monte Carlo Methods* (Wiley, New York, 1965), p. 55.
[55]G. V. Chester, and L. Reatto, Phys. Rev. 155, 88 (1967).
[56]We wish to thank D. Levesque for a private communication on this matter.
[57]G. V. Chester and D. M. Ceperley, Phys. Rev. A 15, 755 (1977).